

$H_0 = 69.8 \pm 1.3 \text{ km s}^{-1} \text{ Mpc}^{-1}$, $\Omega_{m0} = 0.288 \pm 0.017$, and other constraints from lower-redshift, non-CMB, expansion-rate data

Shulei Cao[✉]* and Bharat Ratra^{✉†}

Department of Physics, Kansas State University, 116 Cardwell Hall, Manhattan, Kansas 66506, USA



(Received 27 February 2023; accepted 2 May 2023; published 17 May 2023)

We use updated type Ia Pantheon + supernova, baryon acoustic oscillation, and Hubble parameter (now also accounting for correlations) data, as well as new reverberation-measured C IV quasar data, and quasar angular size, H II starburst galaxy, reverberation-measured Mg II quasar, and Amati-correlated gamma-ray burst data to constrain cosmological parameters. We show that these datasets result in mutually consistent constraints and jointly use them to constrain cosmological parameters in six different spatially flat and nonflat cosmological models. Our analysis provides summary model-independent determinations of two key cosmological parameters: the Hubble constant, $H_0 = 69.8 \pm 1.3 \text{ km s}^{-1} \text{ Mpc}^{-1}$, and the current nonrelativistic matter density parameter, $\Omega_{m0} = 0.288 \pm 0.017$. Our summary error bars are 2.4 and 2.3 times those obtained using the flat cosmological constant cold dark matter (Λ CDM) model and *Planck* TT, TE, EE + lowE + lensing cosmic microwave background (CMB) anisotropy data. Our H_0 value is very consistent with that from the local expansion rate based on the tip of the red giant branch and type Ia supernova (SN Ia) data, is 2σ lower than that from the local expansion rate based on Cepheid and SN Ia data, and is 2σ higher than that in the flat Λ CDM model based on *Planck* TT, TE, EE + lowE + lensing CMB data. Our data compilation shows at most mild evidence for nonflat spatial hypersurfaces, but more significant evidence for dark energy dynamics, 2σ or larger in the spatially flat dynamical dark energy models we study.

DOI: 10.1103/PhysRevD.107.103521

I. INTRODUCTION

The Universe is currently expanding at an increasing rate, a finding supported by a number of observations. The most widely accepted explanation for this acceleration is dark energy, a hypothetical substance with negative pressure. In the spatially flat cosmological constant cold dark matter (Λ CDM) model, [1], dark energy is taken to be a cosmological constant and contributes about 70% of the total energy budget of the current Universe. However, recent observations may indicate potential discrepancies with this model [2–6] and have led to the exploration of alternate models that allow for nonzero spatial curvature and dark energy dynamics. In our analyses here, we also explore some of these alternatives.

Cosmological models have been compared and cosmological parameter constraints have been determined using various observations, including cosmic microwave background (CMB) anisotropy data [7], that probe the high-redshift Universe, and lower-redshift expansion-rate observations like those we use here. These lower-redshift datasets include better-established probes such as Hubble parameter [$H(z)$] data that reach to redshift $z \sim 2$, and

baryon acoustic oscillation (BAO) and type Ia supernova (SN Ia) measurements that reach to $z \sim 2.3$ [8–10], as well as emerging probes such as H II starburst galaxy (H II G) apparent magnitude data that reach to $z \sim 2.5$ [11–16], quasar angular size (QSO-AS) measurements that reach to $z \sim 2.7$ [17–21], reverberation-measured (RM) Mg II and C IV quasar (QSO) measurements that reach to $z \sim 3.4$ [22–28], and gamma-ray burst (GRB) data that reach to $z \sim 8.2$ [29–39], of which only 118 Amati-correlated (A118) GRBs, with lower intrinsic dispersion, are suitable for cosmological purposes [37,40–43].

In our analyses here, we also exclude RM H β QSO data that probe to $z \sim 0.9$ [22,23,44], because the resulting cosmological parameter constraints are in $\sim 2\sigma$ tension with those from more established probes. QSO flux observations that reach to $z \sim 7.5$ have been studied [45–55]; however, we also exclude these QSOs from our analyses here since the latest QSO flux compilation [50] is not standardizable [51,52,56,57].

We use only the above-listed, not unreliable, lower-redshift ($z \leq 8.2$) expansion-rate datasets to derive cosmological parameter constraints. This is because we want to derive constraints that are independent of CMB anisotropy data that result in constraints that contradict some local distance-ladder measurements of the Hubble constant H_0 , [2–6]. We also do not use growth-rate data here, since the use of such data requires assumption of a

*shulei@phys.ksu.edu

†ratra@phys.ksu.edu

primordial inhomogeneity power spectrum and so additional freedom.

We emphasize, as discussed below, that we do use SN Ia that are also used in distance-ladder H_0 measurements, but unlike in the distance-ladder case, we do not use, e.g., Cepheid or tip of the red giant branch (TRGB) distances to calibrate SN Ia data. We also note, as discussed below, that the H II G data we use assume a correlation relation that is calibrated by using a compilation of Cepheid, TRGB, and other data; in the Appendix, we discuss cosmological constraints that do not make use of the H II G measurements and so are independent of both CMB data and more conventional distance-ladder data.

In this paper, we build and improve upon our earlier work in Ref. [58]. In particular, we use new Pantheon + SN Ia (SNP+) data, update our BAO data compilation, and update as well as now account for the correlations between some of the $H(z)$ measurements. We now also include new RM C IV QSO data and now also more correctly account for the asymmetric errors in RM Mg II QSO and C IV QSO data. We show that the results from each of the individual datasets are mutually consistent and also show that the updated joint results do not differ significantly from the joint results of Ref. [58]. In particular, our joint analysis of new $H(z)$ + BAO + SNP+ + QSO-AS + HII G + Mg II + CIV + A118 data here yields summary model-independent values of the nonrelativistic matter density parameter $\Omega_{m0} = 0.288 \pm 0.017$ and $H_0 = 69.8 \pm 1.3 \text{ km s}^{-1} \text{ Mpc}^{-1}$, which are 0.29σ lower and 0.057σ higher than the summary joint constraints from Ref. [58], $\Omega_{m0} = 0.295 \pm 0.017$ and $H_0 = 69.7 \pm 1.2 \text{ km s}^{-1} \text{ Mpc}^{-1}$.

Our $H_0 = 69.8 \pm 1.3 \text{ km s}^{-1} \text{ Mpc}^{-1}$ measurement is in better agreement with the median statistics $H_0 = 68 \pm 2.8 \text{ km s}^{-1} \text{ Mpc}^{-1}$ estimate of Ref. [59] and the TRGB and SN Ia local expansion rate $H_0 = 69.8 \pm 1.7 \text{ km s}^{-1} \text{ Mpc}^{-1}$ estimate of Ref. [60] than with the Cepheids and SN Ia local expansion rate $H_0 = 73.04 \pm 1.04 \text{ km s}^{-1} \text{ Mpc}^{-1}$ estimate of Ref. [61] and the flat Λ CDM model $H_0 = 67.36 \pm 0.54 \text{ km s}^{-1} \text{ Mpc}^{-1}$ estimate from *Planck* 2018 TT, TE, EE + lowE + lensing CMB anisotropy data [7], differing by $\sim 2\sigma$ from the last two. (As discussed in the Appendix, excluding H II G data results in H_0 values that are $\sim 0.9\sigma$ higher than the *Planck* flat Λ CDM model value and $\sim 1.3\text{--}1.6\sigma$ lower than the Cepheids and SN Ia local expansion rate value of Ref. [61].) These data show at most mild evidence for nonflat spatial hypersurfaces, but more significant evidence for dark energy dynamics, 2σ or larger in the spatially flat dynamical dark energy models we study. Based on the deviance information criterion, flat ϕ CDM is the most favored cosmological model.

This paper is organized as follows. In Sec. II, we summarize the cosmological models and parametrizations used in our analyses. Section III provides a detailed description of the datasets used in our analyses. The methods we employ are summarized in Sec. IV. In

Sec. V, we present our findings on the constraints of cosmological parameters. We summarize our conclusions in Sec. VI. Constraints that do not make use of H II G data are discussed in the Appendix.

II. COSMOLOGICAL MODELS

We use six cosmological models to study the datasets we consider. These data are used to constrain the parameters of the six cosmological models that apply for different combinations of flat or nonflat spatial geometry and a constant cosmological constant or a dynamical dark energy density. For recent determinations of constraints on spatial curvature, see Refs. [62–84] and references therein. We compare the goodness of fit of these models. We use multiple, potentially very different, cosmological models in order to be able to determine which cosmological parameters are constrained in a model-independent manner by the datasets we use.

To compute cosmological parameter constraints in these models, we use the Hubble parameter, $H(z, \mathbf{p})$, which is a function of the redshift z and the cosmological parameters \mathbf{p} in the given model. The Hubble parameter is related to the expansion rate function and the Hubble constant as $H(z, \mathbf{p}) = H_0 E(z, \mathbf{p})$. In these models, we assume the presence of one massive and two massless neutrino species, with the total neutrino mass ($\sum m_\nu$) being 0.06 eV and an effective number of relativistic neutrino species of $N_{\text{eff}} = 3.046$. This allows us to compute the current nonrelativistic matter density parameter value, Ω_{m0} , from the current values of the physical energy density parameters for nonrelativistic neutrinos ($\Omega_\nu h^2$), baryons ($\Omega_b h^2$), and cold dark matter ($\Omega_c h^2$), and the Hubble constant h in units of $100 \text{ km s}^{-1} \text{ Mpc}^{-1}$, as $\Omega_{m0} = (\Omega_\nu h^2 + \Omega_b h^2 + \Omega_c h^2)/h^2$, where $\Omega_\nu h^2 = \sum m_\nu/(93.14 \text{ eV})$ is a constant.

In the flat and nonflat Λ CDM models, the expansion rate function is

$$E(z, \mathbf{p}) = \sqrt{\Omega_{m0}(1+z)^3 + \Omega_{k0}(1+z)^2 + \Omega_\Lambda}, \quad (1)$$

where the current value of the spatial curvature energy density parameter $\Omega_{k0} = 0$ in flat Λ CDM and the cosmological constant dark energy density parameter $\Omega_\Lambda = 1 - \Omega_{m0} - \Omega_{k0}$. The cosmological parameters being constrained are $\mathbf{p} = \{H_0, \Omega_b h^2, \Omega_c h^2\}$ and $\mathbf{p} = \{H_0, \Omega_b h^2, \Omega_c h^2, \Omega_{k0}\}$ in the flat and nonflat Λ CDM models, respectively.

In the flat and nonflat XCDM parametrizations,

$$E(z, \mathbf{p}) = \sqrt{\Omega_{m0}(1+z)^3 + \Omega_{k0}(1+z)^2 + \Omega_{X0}(1+z)^{3(1+w_X)}}, \quad (2)$$

where the current value of the X-fluid dynamical dark energy density parameter $\Omega_{X0} = 1 - \Omega_{m0} - \Omega_{k0}$ and the X-fluid (dark energy) equation of state parameter

$w_X = p_X/\rho_X$ is allowed to take values different from -1 (which corresponds to a cosmological constant), and where p_X and ρ_X are the pressure and energy density of the X-fluid, respectively. The cosmological parameters being constrained are $\mathbf{p} = \{H_0, \Omega_b h^2, \Omega_c h^2, w_X\}$ and $\mathbf{p} = \{H_0, \Omega_b h^2, \Omega_c h^2, w_X, \Omega_{k0}\}$ in the flat and nonflat XCDM parametrizations, respectively. Discussions of parametrizations of dynamical dark energy may be traced through Refs. [85–87].

In the flat and nonflat ϕ CDM models [88–90],

$$E(z, \mathbf{p}) = \sqrt{\Omega_{m0}(1+z)^3 + \Omega_{k0}(1+z)^2 + \Omega_\phi(z, \alpha)}, \quad (3)$$

where the scalar field (ϕ) dynamical dark energy density parameter is

$$\Omega_\phi(z, \alpha) = \frac{1}{6H_0^2} \left[\frac{1}{2} \dot{\phi}^2 + V(\phi) \right], \quad (4)$$

which is determined by numerically solving the Friedmann equation (3) and the equation of motion of the scalar field,

$$\ddot{\phi} + 3H\dot{\phi} + V'(\phi) = 0, \quad (5)$$

with an overdot and a prime denoting a derivative with respect to time and ϕ , respectively. Here, we assume an inverse power-law scalar field potential energy density,

$$V(\phi) = \frac{1}{2} \kappa m_p^2 \phi^{-\alpha}, \quad (6)$$

where m_p is the Planck mass, α is a positive constant ($\alpha = 0$ corresponds to a cosmological constant), and κ is a constant that is determined by the shooting method in the cosmic linear anisotropy solving system (CLASS) code [91]. The cosmological parameters being constrained are $\mathbf{p} = \{H_0, \Omega_b h^2, \Omega_c h^2, \alpha\}$ and $\mathbf{p} = \{H_0, \Omega_b h^2, \Omega_c h^2, \alpha, \Omega_{k0}\}$ in the flat and nonflat ϕ CDM models, respectively. For recent studies on constraints on ϕ CDM, see Refs. [92–106] and related references within these papers.

Note that in analyses of some of the datasets we use, we set $H_0 = 70 \text{ km s}^{-1} \text{ Mpc}^{-1}$ and $\Omega_b = 0.05$, with \mathbf{p} changing accordingly, because these data are unable to constrain H_0 and Ω_b .

III. DATA

In this paper, compared to the data we used in Ref. [58], we now use updated $H(z)$ data and an improved $H(z)$ analysis that now includes the covariance matrix for a subset of these data from Refs. [107], updated BAO data, new Pantheon + SN Ia data, an improved analysis of reverberation measured Mg II QSO data, and new reverberation measured C IV QSO data, as well as other datasets, to constrain cosmological parameters. We also correct an

error in one GRB measurement used in Ref. [58], as discussed below. These data are summarized next.

$H(z)$ data. The 32 $H(z)$ measurements listed in Table I have a redshift range of $0.07 \leq z \leq 1.965$. The covariance matrix of the 15 correlated measurements originally from Refs. [109–111], discussed in Ref. [107], can be found at [108]. In the following, we refer to the $H(z)$ dataset used in Ref. [58] as old $H(z)$ data.

BAO data. The 12 BAO measurements listed in Table II cover the redshift range $0.122 \leq z \leq 2.334$. The quantities listed in Table II are described as follows:

- (i) $D_V(z)$: Spherically averaged BAO distance, $D_V(z) = [cz(1+z)^2 H(z)^{-1} D_A^2(z)]^{1/3}$, where c is the speed of light and the angular diameter distance $D_A(z) = D_M(z)/(1+z)$ with $D_M(z)$ defined in the following:
- (ii) $D_H(z)$: Hubble distance, $D_H(z) = c/H(z)$
- (iii) r_s : Sound horizon at the drag epoch, $r_{s,\text{fid}} = 147.5 \text{ Mpc}$ in Ref. [112]

TABLE I. 32 $H(z)$ data.

z	$H(z)$ ^a	Reference
0.07	69.0 ± 19.6	[125]
0.09	69.0 ± 12.0	[126]
0.12	68.6 ± 26.2	[125]
0.17	83.0 ± 8.0	[126]
0.2	72.9 ± 29.6	[125]
0.27	77.0 ± 14.0	[126]
0.28	88.8 ± 36.6	[125]
0.4	95.0 ± 17.0	[126]
0.47	89.0 ± 50.0	[127]
0.48	97.0 ± 62.0	[128]
0.75	98.8 ± 33.6	[129]
0.88	90.0 ± 40.0	[128]
0.9	117.0 ± 23.0	[126]
1.3	168.0 ± 17.0	[126]
1.43	177.0 ± 18.0	[126]
1.53	140.0 ± 14.0	[126]
1.75	202.0 ± 40.0	[126]
0.1791	74.91	[107] ^b
0.1993	74.96	[107] ^b
0.3519	82.78	[107] ^b
0.3802	83.0	[107] ^b
0.4004	76.97	[107] ^b
0.4247	87.08	[107] ^b
0.4497	92.78	[107] ^b
0.4783	80.91	[107] ^b
0.5929	103.8	[107] ^b
0.6797	91.6	[107] ^b
0.7812	104.5	[107] ^b
0.8754	125.1	[107] ^b
1.037	153.7	[107] ^b
1.363	160.0	[107] ^b
1.965	186.5	[107] ^b

^a $\text{km s}^{-1} \text{ Mpc}^{-1}$.

^bThese 15 measurements are correlated and used in our analyses with a full covariance matrix as noted in Sec. III.

(iv) $D_M(z)$: Transverse comoving distance,

$$D_M(z) = \begin{cases} \frac{c}{H_0\sqrt{\Omega_{k0}}} \sinh \left[\frac{H_0\sqrt{\Omega_{k0}}}{c} D_C(z) \right] & \text{if } \Omega_{k0} > 0, \\ D_C(z) & \text{if } \Omega_{k0} = 0, \\ \frac{c}{H_0\sqrt{|\Omega_{k0}|}} \sin \left[\frac{H_0\sqrt{|\Omega_{k0}|}}{c} D_C(z) \right] & \text{if } \Omega_{k0} < 0, \end{cases} \quad (7)$$

where the comoving distance

$$D_C(z) = c \int_0^z \frac{dz'}{H(z')} \cdot \quad (8)$$

The covariance matrices for given BAO data are as follows. The covariance matrix \mathbf{C} for BAO data from Ref. [113] is

$$\begin{bmatrix} 1.3225 & -0.1009 \\ -0.1009 & 0.0380 \end{bmatrix}, \quad (9)$$

for BAO data from Ref. [114] it is

$$\begin{bmatrix} 0.02860520 & -0.04939281 & 0.01489688 & -0.01387079 \\ 0.04939281 & -0.5307187 & -0.02423513 & 0.1767087 \\ 0.01489688 & -0.02423513 & 0.04147534 & -0.04873962 \\ -0.01387079 & 0.1767087 & -0.04873962 & 0.3268589 \end{bmatrix}, \quad (10)$$

for BAO data from Refs. [114,115], it is

$$\begin{bmatrix} 0.1076634008565565 & -0.05831820341302727 \\ -0.05831820341302727 & 0.2838176386340292 \end{bmatrix}, \quad (11)$$

TABLE II. 12 BAO data.

z	Measurement ^a	Value	Reference
0.122	$D_V(r_{s,\text{fid}}/r_s)$	539 ± 17	[112]
0.38	D_M/r_s	10.23406	[114] ^b
0.38	D_H/r_s	24.98058	[114] ^b
0.51	D_M/r_s	13.36595	[114] ^b
0.51	D_H/r_s	22.31656	[114] ^b
0.698	D_M/r_s	17.85823691865007	[114, 115] ^c
0.698	D_H/r_s	19.32575373059217	[114, 115] ^c
0.835	D_M/r_s	18.92 ± 0.51	[130] ^d
1.48	D_M/r_s	30.6876	[116, 117] ^e
1.48	D_H/r_s	13.2609	[116, 117] ^e
2.334	D_M/r_s	37.5	[113] ^f
2.334	D_H/r_s	8.99	[113] ^f

^a $D_V, r_s, r_{s,\text{fid}}, D_M, D_H$, and D_A have units of Mpc.

^bThe four measurements from Ref. [114] are correlated; see Eq. (10) below for their correlation matrix.

^cThe two measurements from Refs. [114,115] are correlated; see Eq. (11) below for their correlation matrix.

^dThis measurement is updated relative to the one from Ref. [131] used in Ref. [58].

^eThe two measurements from Refs. [116,117] are correlated; see Eq. (12) below for their correlation matrix.

^fThe two measurements from Ref. [113] are correlated; see Eq. (9) below for their correlation matrix.

and for BAO data from Refs. [116,117], it is

$$\begin{bmatrix} 0.63731604 & 0.1706891 \\ 0.1706891 & 0.30468415 \end{bmatrix}. \quad (12)$$

In the following, we refer to the BAO data compilation used in Ref. [58] as old BAO data. As discussed, e.g., below Eq. (45) of Ref. [115], BAO measurements are robust to the choice of fiducial cosmology, close to the assumed one.

SN Ia data. We used two sets of SN Ia data jointly in the analyses of Ref. [58]: 1048 Pantheon (abbreviated as “SNP”) measurements from Ref. [118] that span a redshift range of $0.01 < z < 2.3$ and 20 binned DES 3 yr (abbreviated as “SND”) measurements from Ref. [119] that span a redshift range of $0.015 \leq z \leq 0.7026$. In the following, we refer to the SN Ia data compilation used in Ref. [58] as SNP + SND data. In this paper, we use 1590 of the 1701 Pantheon + SN Ia (abbreviated as “SNP+”) measurements from Ref. [10] that span a redshift range of $0.01016 \leq z \leq 2.26137$, with a minimum redshift of $z > 0.01$ to avoid dependence on peculiar velocity models.

We note that SNP + data includes updated SNP and SND data.

QSO angular size (QSO-AS) data. The 120 QSO angular size measurements are listed in Table 1 of Ref. [17] and span the redshift range 0.462 ≤ z ≤ 2.73. The angular size of a QSO can be predicted in a given cosmological model by using the formula $\theta(z) = l_m/D_A(z)$, where l_m is the characteristic linear size of the QSOs in the sample and $D_A(z)$ is the angular diameter distance at redshift z .

H II G data. The 181 H II G measurements listed in Table A3 of Ref. [13] include 107 low- z ones from Ref. [12] recalibrated in Ref. [120], spanning the redshift range 0.0088 ≤ z ≤ 0.16417, and 74 high- z ones spanning the redshift range 0.63427 ≤ z ≤ 2.545. These sources follow a correlation between the observed luminosity (L) of the Balmer emission lines and the velocity dispersion (σ) of the ionized gas, represented by the equation $\log L = \beta \log \sigma + \gamma$, where $\log = \log_{10}$. In Ref. [13], 107 low- z H II G and 36 giant extragalactic H II regions (GH II R) data are used to determine the intercept and slope parameters, β and γ , which are found to be 5.022 ± 0.058 and 33.268 ± 0.083 , respectively. To infer the distances for GH II R data, they relied on primary indicators such as Cepheids, TRGB, and theoretical model calibrations, [121]. Using this relation, the observed distance modulus of an H II G can be computed as $\mu_{\text{obs}} = 2.5 \log L - 2.5 \log f - 100.2$, where $f(z)$ is the measured flux at redshift z corrected for extinction using the Gordon extinction law [122]. The theoretical distance modulus in a given cosmological model is $\mu_{\text{th}}(z) = 5 \log D_L(z) + 25$, where $D_L(z) = (1+z)D_M(z)$ is the luminosity distance.

Mg II QSO and C IV QSO sample. The sample of 78 Mg II QSO and 38 C IV QSO measurements, listed in Tables A1 of Refs. [25,27], respectively, span a wide range of redshifts, from 0.0033 ≤ z ≤ 1.89 for Mg II QSOs and from 0.001064 ≤ z ≤ 3.368 for C IV QSOs. Both Mg II QSO and C IV QSO sources follow the radius-luminosity ($R - L$) relation $\log \tau = \beta + \gamma(\log L - 44)$. Here, τ (days) is the QSO time-lag, β is the intercept parameter, and γ is the slope parameter. For Mg II QSOs and C IV QSOs, we denote β and γ as β_M and γ_M , and β_C and γ_C , respectively. The monochromatic luminosity $L = 4\pi D_L^2 F$, where F is the QSO flux measured in units of erg s⁻¹ cm⁻² at 1350 Å and 3000 Å for Mg II QSOs and C IV QSOs, respectively. As described in Refs. [25,27], in our analysis, we must simultaneously determine both $R - L$ relation and cosmological parameters and verify that the $R - L$ relation parameters are independent of the assumed cosmological model for the Mg II QSOs and C IV QSOs to be standardizable. In addition to what we used in

Ref. [58], here we also use the 38 C IV QSOs and improve on the analyses of these QSOs by now accounting for the asymmetry in the data error bars, as described in Ref. [27].

A118 GRB sample. The A118 sample, which is listed in Table 7 of Ref. [37], consists of 118 long GRBs and spans a wide redshift range, from 0.3399 to 8.2. The isotropic radiated energy E_{iso} of a GRB source in its rest frame is $E_{\text{iso}} = 4\pi D_L^2 S_{\text{bolo}}/(1+z)$, where S_{bolo} is the bolometric fluence computed in the standard rest-frame energy band 1–10⁴ keV. The peak energy of a source is $E_p = (1+z)E_{p,\text{obs}}$, where $E_{p,\text{obs}}$ is the observed peak energy. There is a correlation between E_{iso} and E_p known as the Amati correlation [123,124], which is given by $\log E_{\text{iso}} = \beta_A + \gamma_A \log E_p$. As described in Ref. [37], we must simultaneously determine both the Amati relation and cosmological parameters and verify that the Amati relation parameters are independent of the assumed cosmological model for the A118 GRBs to be standardizable. Note that here we use the correct value of $E_p = 871 \pm 123$ keV for GRB081121, as discussed in Ref. [43], rather than the value listed in Table 7 of Ref. [37] and used in Ref. [58].

IV. DATA ANALYSIS METHODOLOGY

The natural log of the likelihood function for the C IV, Mg II, and A118 datasets (denoted with subscript “s” that is either C IV, Mg II, or A118) with measured quantity \mathbf{Q} , [132], is

$$\ln \mathcal{L}_s = -\frac{1}{2} \left[\chi_s^2 + \sum_{i=1}^N \ln (2\pi\sigma_{\text{tot},s,i}^2) \right], \quad (13)$$

where

$$\chi_s^2 = \sum_{i=1}^N \left[\frac{(\mathbf{Q}_{\text{obs},s,i} - \mathbf{Q}_{\text{th},s,i})^2}{\sigma_{\text{tot},s,i}^2} \right] \quad (14)$$

with a total uncertainty,

$$\sigma_{\text{tot},s,i}^2 = \sigma_{\text{int},s}^2 + \sigma_{\mathbf{Q}_{\text{obs},s,i}}^2 + \sigma_{\mathbf{Q}_{\text{th},s,i}}^2. \quad (15)$$

$\sigma_{\text{int},s}$ represents the intrinsic scatter parameter for data s, which also accounts for unknown systematic uncertainties. N is the total number of data points.

The natural log of the likelihood function for some $H(z)$ and BAO data and for QSO-AS and H II G data (also denoted “s”) with measured quantity \mathbf{Q} is

$$\ln \mathcal{L}_s = -\frac{1}{2} \chi_s^2, \quad (16)$$

where

$$\chi_s^2 = \sum_{i=1}^N \left[\frac{(\mathbf{Q}_{\text{obs},s,i} - \mathbf{Q}_{\text{th},s,i})^2}{\sigma_{\text{tot},s,i}^2} \right] \quad (17)$$

with a total uncertainty,

$$\sigma_{\text{tot},s,i}^2 = \sigma_{\text{sys},s,i}^2 + \sigma_{\mathbf{Q}_{\text{obs},s,i}}^2 + \sigma_{\mathbf{Q}_{\text{th},s,i}}^2, \quad (18)$$

with $\sigma_{\text{sys},s,i}$ being the systematic uncertainty at redshift z_i . It is important to note that we have ignored the systematic uncertainties for H II G data because they are not yet properly quantified. Following Ref. [17], the total uncertainty for QSO-AS data is calculated as $\sigma_{\text{tot},i} = \sigma_{\theta_{\text{obs},i}} + 0.1\theta_{\text{obs},i}$, taking into consideration a 10% margin for both observational and intrinsic errors in the observed angular sizes $\theta_{\text{obs},i}$.

For those $H(z)$ and BAO data (also denoted “s”) with covariance matrix \mathbf{C}_s ,

$$\chi_s^2 = [\mathbf{Q}_{\text{th},s,i} - \mathbf{Q}_{\text{obs},s,i}]^T \mathbf{C}_s^{-1} [\mathbf{Q}_{\text{th},s,i} - \mathbf{Q}_{\text{obs},s,i}], \quad (19)$$

in which superscripts T and -1 represent transpose and inverse of the matrix, respectively.

For SN Ia data, χ_{SN}^2 is calculated using Eq. (C1) in Appendix C of Ref. [133]. In this equation, the variable \mathcal{M} , that includes the SN Ia absolute magnitude M and the Hubble constant H_0 , is marginalized; therefore, here SN Ia data cannot constrain H_0 . However, when we allow $\Omega_b h^2$ and $\Omega_c h^2$ to be free parameters, H_0 is derived from the $\Omega_b h^2$ and $\Omega_c h^2$ constraints.

In this paper, we do not use CMB data. Instead, in our analyses of BAO data, we determine the sound horizon r_s by also constraining $\Omega_b h^2$ and $\Omega_c h^2$ from these data. Consequently, our cosmological parameter constraints do not depend on CMB data.

The QSO-AS + H II G and Mg II + C IV constraints used in our paper are taken from Refs. [27,58], respectively. The analyses of Ref. [27] account for the asymmetric errors of the Mg II + C IV measurements.

The flat priors for the free cosmological and noncosmological parameters are listed in Table III. Some of the individual datasets (or smaller combinations of individual datasets) are unable to constrain some cosmological parameters. In these cases, we fix these cosmological parameter values; see discussion in Table III footnotes. Note that we do not need to do this for larger combinations of individual datasets; these data combinations determine cosmological parameter values in a prior-independent manner.

The Markov chain Monte Carlo (MCMC) code MontePython [134,135] is utilized to maximize the likelihood functions and determine the posterior distributions of all free parameters. The PYTHON package GetDist [136] is used to analyze the MCMC results and create plots.

TABLE III. Flat priors of the constrained parameters.

Parameter	Prior
Cosmological parameters	
h^a	[None, None]
$\Omega_b h^{2b}$	[0, 1]
$\Omega_c h^{2c}$	[0, 1]
Ω_{k0}	[-2, 2]
α	[0, 10]
w_X	[-5, 0.33]
Noncosmological parameters	
γ_M	[0, 5]
β_M	[0, 10]
$\sigma_{\text{int},M}$	[0, 5]
γ_C	[0, 5]
β_C	[0, 10]
$\sigma_{\text{int},C}$	[0, 5]
γ_A	[0, 5]
β_A	[0, 300]
$\sigma_{\text{int},A}$	[0, 5]
l_m	[None, None]

^a H_0 in unit of $100 \text{ km s}^{-1} \text{ Mpc}^{-1}$. In the Mg II + C IV and A118 cases $h = 0.7$, in the SNP + SND and SNP + cases $0.2 \leq h \leq 1$, and in other cases, the h prior range is irrelevant (unbounded).

^bIn the Mg II + C IV and A118 cases $\Omega_b h^2$ is set to be 0.0245, i.e., $\Omega_b = 0.05$.

^cIn the Mg II + C IV and A118 cases $\Omega_{m0} \in [0, 1]$ is ensured.

The Akaike information criterion (AIC), the Bayesian information criterion (BIC), and the deviance information criterion (DIC) are

$$\text{AIC} = -2 \ln \mathcal{L}_{\text{max}} + 2n, \quad (20)$$

$$\text{BIC} = -2 \ln \mathcal{L}_{\text{max}} + n \ln N, \quad (21)$$

and

$$\text{DIC} = -2 \ln \mathcal{L}_{\text{max}} + 2n_{\text{eff}}, \quad (22)$$

where n is the number of parameters in the given model, and $n_{\text{eff}} = \langle -2 \ln \mathcal{L} \rangle + 2 \ln \mathcal{L}_{\text{max}}$ represents the number of effectively constrained parameters. Here, the angular brackets indicate an average over the posterior distribution and \mathcal{L}_{max} is the maximum value of the likelihood function.

$\Delta A/B/DIC$ values are computed by subtracting the $\Delta A/B/DIC$ value of the flat Λ CDM reference model from the values of the other five cosmological dark energy models. Negative values of $\Delta A/B/DIC$ indicate that the model being evaluated fits the dataset better than does the flat Λ CDM reference model, while positive values indicate a worse fit. In comparison to the model with the lowest $A/B/DIC$ value, a $\Delta A/B/DIC$ value within the range (0, 2] indicates weak evidence against the model being evaluated, a value within (2, 6] indicates positive

TABLE IV. Unmarginalized best-fitting parameter values for all models from various combinations of BAO, $H(z)$, and SN Ia data.

Model	Dataset	$\Omega_b h^2$	$\Omega_c h^2$	Ω_{m0}	Ω_{k0}	w_X/α^a	H_0^b	$-2 \ln \mathcal{L}_{\max}$	AIC	BIC	DIC	ΔAIC	ΔBIC	ΔDIC
Flat Λ CDM	Old $H(z)$	0.0273	0.1201	0.319	68.16	14.54	20.54	24.94	18.87	0.00	0.00	0.00
	$H(z)$	0.0120	0.1366	0.309	69.43	14.50	20.50	24.90	18.78	0.00	0.00	0.00
	Old $H(z)$ + old BAO	0.0244	0.1181	0.301	68.98	25.64	31.64	36.99	32.32	0.00	0.00	0.00
	$H(z)$ + BAO	0.0254	0.1200	0.297	70.12	30.56	36.56	41.91	37.32	0.00	0.00	0.00
	SNP + SND	0.0102	0.0133	0.309	27.93	1056.64	1062.64	1077.56	1058.68	0.00	0.00	0.00
	SNP +	0.0139	0.1031	0.331	59.59	1406.97	1412.97	1429.08	1409.17	0.00	0.00	0.00
	Old $H(z)$ + old BAO + SNP + SND	0.0242	0.1191	0.304	68.86	1082.39	1088.39	1103.44	1089.92	0.00	0.00	0.00
	$H(z)$ + BAO + SNP +	0.0239	0.1256	0.312	69.35	1439.59	1445.59	1461.79	1446.05	0.00	0.00	0.00
Nonflat Λ CDM	Old $H(z)$	0.0205	0.1515	0.362	-0.136	...	69.09	14.49	22.49	28.36	20.19	1.96	3.42	1.32
	$H(z)$	0.0180	0.1328	0.314	-0.012	...	69.47	14.50	22.50	28.37	20.09	2.00	3.47	1.31
	Old $H(z)$ + old BAO	0.0260	0.1098	0.292	0.048	...	68.35	25.30	33.30	40.43	33.87	1.66	3.44	1.54
	$H(z)$ + BAO	0.0269	0.1128	0.289	0.041	...	69.61	30.34	38.34	45.48	38.80	1.78	3.56	1.48
	SNP + SND	0.0335	0.1292	0.326	-0.043	...	70.84	1056.58	1064.58	1084.47	1060.96	1.94	6.91	2.28
	SNP +	0.0336	0.0663	0.295	0.095	...	58.43	1406.46	1414.46	1435.95	1410.81	1.49	6.87	1.65
	Old $H(z)$ + Old BAO + SNP + SND	0.0255	0.1121	0.295	0.035	...	68.53	1082.11	1090.11	1110.16	1091.17	1.72	6.72	1.24
	$H(z)$ + BAO + SNP +	0.0276	0.1078	0.288	0.084	...	68.69	1437.61	1445.61	1467.21	1446.04	0.02	5.42	-0.01
Flat XCDM	Old $H(z)$	0.0376	0.1236	0.321	...	-1.261	70.95	14.39	22.39	28.25	22.17	1.85	3.32	3.30
	$H(z)$	0.0106	0.1464	0.316	...	-1.140	70.63	14.47	22.47	28.33	22.28	1.97	3.43	3.49
	Old $H(z)$ + old BAO	0.0296	0.0951	0.290	...	-0.754	65.79	22.39	30.39	37.52	30.63	-1.25	0.53	-1.69
	$H(z)$ + BAO	0.0318	0.0938	0.283	...	-0.734	66.67	26.58	34.58	41.71	34.83	-1.98	-0.20	-2.49
	SNP + SND	0.0162	0.1648	0.319	...	-1.028	75.45	1056.62	1064.62	1084.52	1061.01	1.98	6.96	2.33
	SNP +	0.0243	0.0745	0.288	...	-0.895	58.73	1406.52	1414.52	1436.00	1410.84	1.55	6.92	1.67
	Old $H(z)$ + Old BAO + SNP + SND	0.0258	0.1115	0.295	...	-0.940	68.37	1081.34	1089.34	1109.40	1090.43	0.95	5.96	0.50
	$H(z)$ + BAO + SNP +	0.0283	0.1092	0.290	...	-0.883	68.96	1434.63	1442.63	1464.22	1443.28	-2.96	2.43	-2.77
Nonflat XCDM	Old $H(z)$	0.0223	0.0736	0.172	0.324	-2.272	75.05	14.14	24.14	31.47	20.73	3.60	6.53	1.86
	$H(z)$	0.0316	0.0530	0.151	0.378	-2.278	75.06	14.21	24.21	31.54	21.46	3.71	6.64	2.68
	Old $H(z)$ + old BAO	0.0289	0.0985	0.296	-0.053	-0.730	65.76	22.13	32.13	41.05	32.51	0.49	4.06	0.19
	$H(z)$ + BAO	0.0305	0.0998	0.293	-0.084	-0.703	66.79	26.00	36.00	44.92	36.11	-0.56	3.01	-1.21
	SNP + SND	0.0057	0.0965	0.145	-0.576	-0.596	84.24	1056.24	1066.24	1091.11	1064.60	3.60	13.55	5.92
	SNP +	0.0334	0.0649	0.295	0.194	-1.155	57.96	1406.43	1416.43	1443.29	1413.23	3.46	14.21	4.06
	Old $H(z)$ + old BAO + SNP + SND	0.0255	0.1155	0.300	-0.030	-0.922	68.68	1081.28	1091.28	1116.35	1092.47	2.89	12.91	2.55
	$H(z)$ + BAO + SNP +	0.0278	0.1118	0.294	-0.032	-0.865	69.07	1434.46	1444.46	1471.45	1445.42	-1.13	9.66	-0.63

(Table continued)

TABLE IV. (Continued)

Model	Dataset	$\Omega_b h^2$	$\Omega_c h^2$	Ω_{m0}	Ω_{k0}	w_X/α^a	H_0^b	$-2 \ln \mathcal{L}_{\max}$	AIC	BIC	DIC	ΔAIC	ΔBIC	ΔDIC
Flat ϕ CDM	Old $H(z)$	0.0140	0.1341	0.321	...	0.000	68.04	14.54	22.54	28.40	20.81	2.00	3.47	1.94
	$H(z)$	0.0158	0.1335	0.312	...	0.001	69.31	14.51	22.51	28.37	20.05	2.00	3.47	1.27
	Old $H(z) +$ old BAO	0.0330	0.0911	0.278	...	1.018	66.98	22.14	30.14	37.27	29.56	-1.33	0.46	-2.42
	$H(z) +$ BAO	0.0336	0.0866	0.271	...	1.157	66.80	26.50	34.50	41.64	34.15	-2.05	-0.27	-3.17
	SNP + SND	0.0198	0.0089	0.308	...	0.001	30.81	1056.64	1064.64	1084.53	1062.54	2.00	6.98	3.86
	SNP +	0.0132	0.2553	0.279	...	0.399	98.21	1406.50	1414.50	1435.98	1411.49	1.53	6.90	2.33
	Old $H(z) +$ old BAO + SNP + SND	0.0263	0.1097	0.292	...	0.203	68.39	1081.22	1089.22	1109.28	1089.91	0.83	5.84	-0.01
	$H(z) +$ BAO + SNP +	0.0288	0.1060	0.286	...	0.402	68.84	1434.43	1442.43	1464.02	1442.92	-3.16	2.23	-3.14
	Old $H(z)$	0.0213	0.1514	0.365	-0.144	0.036	68.91	14.50	24.50	31.83	21.42	3.96	6.89	2.55
	$H(z)$	0.0358	0.1120	0.310	0.003	0.011	69.18	14.51	24.51	31.84	20.63	4.00	6.94	1.85
Nonflat ϕ CDM	Old $H(z)$	0.0306	0.0920	0.284	-0.058	1.200	65.91	22.05	32.05	40.97	31.30	0.41	3.98	-1.02
	$H(z)$	0.0337	0.0894	0.275	-0.074	1.393	67.16	25.92	35.92	44.84	35.29	-0.64	2.93	-2.03
	Old $H(z) +$ old BAO	0.0283	0.1387	0.251	-0.251	1.107	81.71	1056.40	1066.40	1091.26	1062.52	3.76	13.71	3.84
	$H(z) +$ BAO	0.0140	0.0525	0.297	0.085	0.005	47.56	1406.47	1416.47	1443.32	1411.50	3.50	14.24	2.33
	SNP +	0.0261	0.1119	0.295	-0.023	0.253	68.56	1081.12	1091.12	1116.19	1091.27	2.73	12.75	1.35
	Old $H(z) +$ old BAO + SNP + SND	0.0282	0.1104	0.291	-0.045	0.480	69.13	1434.23	1444.23	1471.22	1444.26	-1.36	9.43	-1.79
	$H(z) +$ BAO + SNP +
	Old $H(z)$
	$H(z)$
	Old $H(z) +$ old BAO + SNP + SND

^a w_X corresponds to flat/nonflat XCDM and α corresponds to flat/nonflat ϕ CDM.
^b $\text{km s}^{-1} \text{Mpc}^{-1}$

evidence against the model, a value within [6, 10] indicates strong evidence against the model, and a value greater than 10 indicates very strong evidence against the model.

V. RESULTS

A. Comparison of constraints obtained from old $H(z)$ data and $H(z)$ data, old $H(z) +$ old BAO data and $H(z) +$ BAO data, and SNP+ SND data and SNP+ data

For old $H(z)$, $H(z)$, old $H(z) +$ old BAO, $H(z) +$ BAO, SNP + SND, and SNP+ data, the best-fitting parameter values, likelihood values, and information criteria values for all models are given in Table IV and the marginalized posterior mean parameter values and uncertainties for all models are listed in Table V. Figures 1–3 show the probability distributions and confidence regions of cosmological parameters, obtained from old $H(z)$ and $H(z)$ data, from old $H(z) +$ old BAO and $H(z) +$ BAO data, and from SNP + SND and SNP+ data, respectively.

Old $H(z)$ data constraints on Ω_{m0} range from $0.193^{+0.056}_{-0.117}$ (nonflat ϕ CDM) to $0.390^{+0.167}_{-0.172}$ (nonflat Λ CDM), with a difference of 1.1σ . In contrast, $H(z)$ data favor values of Ω_{m0} lower by $\lesssim 0.17\sigma$ and ranging from $0.172^{+0.048}_{-0.104}$ (nonflat ϕ CDM) to $0.374^{+0.151}_{-0.210}$ (nonflat Λ CDM), with a difference of 0.94σ .

Old $H(z)$ data constraints on H_0 range from $62.81^{+2.65}_{-3.18}$ $\text{km s}^{-1} \text{Mpc}^{-1}$ (nonflat ϕ CDM) to $79.55^{+7.01}_{-15.05}$ $\text{km s}^{-1} \text{Mpc}^{-1}$ (flat XCDM), with a difference of 1.1σ . In contrast, $H(z)$ data favor values of H_0 higher by $\lesssim 0.36\sigma$ (and with larger error bars), ranging from $64.32^{+3.59}_{-4.04}$ $\text{km s}^{-1} \text{Mpc}^{-1}$ (nonflat ϕ CDM) to $80.96^{+7.59}_{-16.10}$ $\text{km s}^{-1} \text{Mpc}^{-1}$ (flat XCDM), with a difference of 1.0σ .

Old $H(z)$ data constraints on Ω_{k0} are $-0.174^{+0.501}_{-0.491}$, $0.241^{+0.451}_{-0.261}$, and $0.262^{+0.265}_{-0.337}$ for nonflat Λ CDM, XCDM, and ϕ CDM, respectively. In contrast, $H(z)$ data constraints on Ω_{k0} are $-0.136^{+0.564}_{-0.457}$, $0.228^{+0.456}_{-0.267}$, and $0.277^{+0.249}_{-0.331}$ for nonflat Λ CDM, XCDM, and ϕ CDM, which are 0.056σ higher, 0.025σ lower, and 0.035σ higher than those from old $H(z)$ data, respectively. Both old $H(z)$ and $H(z)$ data indicate that closed spatial geometry is mildly favored by nonflat Λ CDM, and that open spatial geometry is mildly favored by nonflat XCDM and nonflat ϕ CDM, but flat hypersurfaces are still within 1σ .

Both old $H(z)$ data and $H(z)$ data indicate a slight preference for dark energy dynamics, with approximately similar evidence for deviation from the Λ CDM models. For $H(z)$ data, for the flat and nonflat XCDM models, the w_X parameter is found to be 0.84σ and 0.68σ lower than -1 , respectively. Similarly, for both the flat and nonflat ϕ CDM models, the α parameter is found to be 1.1σ away from 0.

Old $H(z) +$ old BAO data constraints on Ω_{m0} range from 0.275 ± 0.023 (flat ϕ CDM) to $0.301^{+0.016}_{-0.018}$ (flat Λ CDM), with a difference of 0.89σ . In contrast, $H(z) +$ BAO data

TABLE V. One-dimensional posterior mean parameter values and uncertainties ($\pm 1\sigma$ error bars or 2σ limits) for all models from various combinations of BAO, $H(z)$, and SNIa data.

Model	Dataset	$\Omega_b h^2$	$\Omega_c h^2$	Ω_{m0}	Ω_{k0}	w_X/α^a	H_0^b
Flat Λ CDM	Old $H(z)$	0.0225 \pm 0.0108	0.1264 \pm 0.0207	0.328 $^{+0.052}_{-0.073}$	67.98 \pm 3.24
	$H(z)$	0.0225 \pm 0.0107	0.1275 \pm 0.0208	0.319 $^{+0.050}_{-0.074}$	69.31 \pm 4.25
	Old $H(z)$ + old BAO	0.0247 \pm 0.0030	0.1186 $^{+0.0076}_{-0.0083}$	0.301 $^{+0.016}_{-0.018}$	69.14 \pm 1.85
	$H(z)$ + BAO	0.0260 \pm 0.0040	0.1212 $^{+0.0091}_{-0.0101}$	0.297 $^{+0.015}_{-0.017}$	70.49 \pm 2.74
	SNP + SND	0.0224 \pm 0.0109	0.1658 $^{+0.0927}_{-0.0598}$	0.310 $^{+0.021}_{-0.023}$	>45.87
	SNP +	0.0224 \pm 0.0109	0.1785 $^{+0.1038}_{-0.0623}$	0.332 \pm 0.020	>44.39
	Old $H(z)$ + old BAO + SNP + SND	0.0244 \pm 0.0027	0.1199 \pm 0.0076	0.304 $^{+0.014}_{-0.015}$	69.04 \pm 1.77
	$H(z)$ + BAO + SNP +	0.0243 \pm 0.0034	0.1267 $^{+0.0080}_{-0.0089}$	0.312 \pm 0.013	69.65 \pm 2.48
	Old $H(z)$	0.0223 $^{+0.0109}_{-0.0108}$	0.1685 $^{+0.0736}_{-0.1139}$	0.390 $^{+0.167}_{-0.172}$	-0.174 $^{+0.501}_{-0.491}$...	69.09 $^{+4.70}_{-4.67}$
	$H(z)$	0.0222 \pm 0.0108	0.1612 $^{+0.0691}_{-0.1207}$	0.374 $^{+0.151}_{-0.210}$	-0.136 $^{+0.564}_{-0.457}$...	69.56 $^{+4.89}_{-4.88}$
Nonflat Λ CDM	Old $H(z)$ + old BAO	0.0266 $^{+0.0039}_{-0.0045}$	0.1088 \pm 0.0166	0.291 \pm 0.023	0.059 $^{+0.081}_{-0.091}$...	68.37 \pm 2.10
	$H(z)$ + BAO	0.0275 $^{+0.0046}_{-0.0051}$	0.1131 $^{+0.0180}_{-0.0181}$	0.289 \pm 0.023	0.047 $^{+0.082}_{-0.089}$...	69.81 \pm 2.80
	SNP + SND	0.0224 \pm 0.0107	0.1698 $^{+0.0766}_{-0.0911}$	0.317 \pm 0.068	-0.017 $^{+0.172}_{-0.174}$...	>46.83
	SNP +	0.0224 \pm 0.0107	0.1745 $^{+0.0750}_{-0.0752}$	0.298 \pm 0.056	0.089 \pm 0.132	...	>53.95
	Old $H(z)$ + old BAO + SNP + SND	0.0260 $^{+0.0037}_{-0.0043}$	0.1119 \pm 0.0157	0.294 \pm 0.022	0.040 \pm 0.070	...	68.62 \pm 1.90
	$H(z)$ + BAO + SNP +	0.0282 $^{+0.0046}_{-0.0050}$	0.1082 \pm 0.0152	0.288 \pm 0.021	0.087 \pm 0.063	...	68.89 \pm 2.44
	Old $H(z)$	0.0225 \pm 0.0107	0.1505 $^{+0.0337}_{-0.0206}$	0.285 $^{+0.061}_{-0.075}$...	-1.972 $^{+1.164}_{-0.588}$	79.55 $^{+7.01}_{-15.05}$
	$H(z)$	0.0225 \pm 0.0108	0.1505 $^{+0.0303}_{-0.0200}$	0.278 $^{+0.065}_{-0.081}$...	-2.127 $^{+1.335}_{-0.629}$	80.96 $^{+7.59}_{-16.10}$
	Old $H(z)$ + old BAO	0.0295 $^{+0.0042}_{-0.0050}$	0.0969 $^{+0.0178}_{-0.0152}$	0.289 \pm 0.020	...	-0.784 $^{+0.140}_{-0.107}$	66.22 $^{+2.31}_{-2.54}$
	$H(z)$ + BAO	0.0308 $^{+0.0053}_{-0.0046}$	0.0978 $^{+0.0184}_{-0.0164}$	0.285 \pm 0.019	...	-0.776 $^{+0.130}_{-0.103}$	67.18 \pm 3.18
Flat XCDM	SNP + SND	0.0224 \pm 0.0108	0.1750 $^{+0.0824}_{-0.0980}$	0.315 $^{+0.083}_{-0.057}$...	-1.054 $^{+0.237}_{-0.171}$	>48.66
	SNP +	0.0224 \pm 0.0107	0.1552 $^{+0.0718}_{-0.0909}$	0.281 $^{+0.079}_{-0.061}$...	-0.900 $^{+0.166}_{-0.124}$	>49.26
	Old $H(z)$ + old BAO + SNP + SND	0.0262 $^{+0.0033}_{-0.0037}$	0.1120 \pm 0.0110	0.295 \pm 0.016	...	-0.941 \pm 0.064	68.55 \pm 1.85
	$H(z)$ + BAO + SNP +	0.0287 \pm 0.0044	0.1097 \pm 0.0117	0.290 \pm 0.016	...	-0.886 \pm 0.053	69.15 \pm 2.52

(Table continued)

TABLE V. (Continued)

Model	Dataset	$\Omega_b h^2$	$\Omega_c h^2$	Ω_{m0}	Ω_{k0}	w_X/α^a	H_0^b
Nonflat XCDM	Old $H(z)$	$0.0218^{+0.0075}_{-0.0144}$	$0.0927^{+0.0217}_{-0.0890}$	$0.2238^{+0.055}_{-0.168}$	$0.241^{+0.451}_{-0.261}$	$-2.148^{+1.682}_{-0.776}$	$71.98^{+5.86}_{-11.09}$
	$H(z)$	$0.0218^{+0.0093}_{-0.0119}$	< 0.2364	$0.2238^{+0.054}_{-0.175}$	$0.2228^{+0.456}_{-0.267}$	$-2.149^{+1.673}_{-0.772}$	$73.06^{+6.61}_{-11.48}$
Old $H(z)$ + old BAO		$0.0294^{+0.0047}_{-0.0050}$	$0.0980^{+0.0186}_{-0.0187}$	0.292 ± 0.025	-0.027 ± 0.109	$-0.770^{+0.149}_{-0.098}$	$66.13^{+2.35}_{-2.36}$
$H(z)$ + BAO		$0.0303^{+0.0054}_{-0.0048}$	0.1021 ± 0.0193	0.292 ± 0.024	-0.054 ± 0.103	$-0.757^{+0.135}_{-0.093}$	67.33 ± 2.96
SNP + SND		0.0224 ± 0.0107	$0.1455^{+0.0644}_{-0.0987}$	0.271 ± 0.085	$0.130^{+0.426}_{-0.249}$	$-1.499^{+0.901}_{-0.237}$	> 48.72
SNP +		0.0224 ± 0.0107	$0.1404^{+0.0654}_{-0.0845}$	$0.259^{+0.071}_{-0.063}$	$0.215^{+0.350}_{-0.202}$	$-1.424^{+0.798}_{-0.251}$	> 49.14
Old $H(z)$ + old BAO + SNP + SND		$0.0262^{+0.0037}_{-0.0043}$	0.1119 ± 0.0157	0.295 ± 0.022	-0.001 ± 0.098	$-0.948^{+0.098}_{-0.068}$	68.53 ± 1.90
$H(z)$ + BAO + SNP +		0.0284 ± 0.0047	$0.1115^{+0.0151}_{-0.0165}$	0.293 ± 0.021	-0.017 ± 0.095	$-0.884^{+0.082}_{-0.058}$	69.23 ± 2.53
Flat ϕ CDM	Old $H(z)$	0.0222 ± 0.0107	$0.0642^{+0.0288}_{-0.0432}$	$0.215^{+0.066}_{-0.108}$...	$3.959^{+1.353}_{-3.789}$	$63.95^{+3.01}_{-3.29}$
	$H(z)$	0.0221 ± 0.0108	$0.0620^{+0.0273}_{-0.0440}$	$0.199^{+0.059}_{-0.106}$...	$3.972^{+1.394}_{-3.739}$	$65.80^{+4.12}_{-4.10}$
Old $H(z)$ + old BAO		$0.0320^{+0.0054}_{-0.0041}$	$0.0855^{+0.0175}_{-0.0174}$	0.275 ± 0.023	...	$1.267^{+0.536}_{-0.807}$	$65.47^{+2.22}_{-2.21}$
$H(z)$ + BAO		$0.0326^{+0.0061}_{-0.0030}$	$0.0866^{+0.0197}_{-0.0180}$	$0.272^{+0.024}_{-0.022}$...	$1.271^{+0.507}_{-0.836}$	$66.19^{+2.89}_{-2.88}$
SNP + SND		0.0221 ± 0.0107	$0.0875^{+0.0333}_{-0.0733}$	$0.181^{+0.075}_{-0.076}$...	< 4.052	> 50.07
SNP +		$0.0220^{+0.0100}_{-0.0118}$	$0.0844^{+0.0288}_{-0.0757}$	$0.175^{+0.065}_{-0.092}$...	$1.966^{+0.479}_{-1.907}$	> 50.58
Old $H(z)$ + old BAO + SNP + SND		$0.0278^{+0.0032}_{-0.0039}$	$0.1054^{+0.0117}_{-0.0100}$	0.287 ± 0.017	...	$0.324^{+0.122}_{-0.264}$	68.29 ± 1.78
$H(z)$ + BAO + SNP +		$0.0300^{+0.0047}_{-0.0046}$	0.1040 ± 0.0129	0.282 ± 0.018	...	$0.475^{+0.189}_{-0.265}$	69.01 ± 2.43
Nonflat ϕ CDM	Old $H(z)$	$0.0215^{+0.0090}_{-0.0120}$	$0.0536^{+0.0160}_{-0.0495}$	$0.193^{+0.056}_{-0.117}$	$0.262^{+0.265}_{-0.337}$	$3.911^{+1.188}_{-3.871}$	$62.81^{+2.65}_{-3.18}$
	$H(z)$	$0.0213^{+0.0083}_{-0.0124}$	$0.0481^{+0.0135}_{-0.0452}$	$0.172^{+0.048}_{-0.104}$	$0.277^{+0.249}_{-0.331}$	$4.087^{+1.393}_{-3.890}$	$64.32^{+3.59}_{-4.04}$
Old $H(z)$ + old BAO		$0.0320^{+0.0057}_{-0.0038}$	$0.0865^{+0.0172}_{-0.0198}$	$0.277^{+0.023}_{-0.026}$	$-0.034^{+0.087}_{-0.098}$	$1.360^{+0.584}_{-0.819}$	65.53 ± 2.19
$H(z)$ + BAO		$0.0325^{+0.0064}_{-0.0029}$	$0.0881^{+0.0199}_{-0.0201}$	0.275 ± 0.025	$-0.052^{+0.093}_{-0.087}$	$1.427^{+0.572}_{-0.830}$	66.24 ± 2.88
SNP + SND		0.0223 ± 0.0107	$0.1098^{+0.0426}_{-0.0861}$	$0.212^{+0.080}_{-0.082}$	$-0.026^{+0.126}_{-0.150}$	< 3.067	> 50.82
SNP +		0.0224 ± 0.0107	$0.1113^{+0.0464}_{-0.0758}$	$0.210^{+0.068}_{-0.069}$	$-0.001^{+0.108}_{-0.132}$	$1.282^{+0.290}_{-1.255}$	> 52.64
Old $H(z)$ + old BAO + SNP + SND		$0.0271^{+0.0038}_{-0.0043}$	0.1095 ± 0.0152	0.292 ± 0.022	$-0.038^{+0.071}_{-0.085}$	$0.382^{+0.151}_{-0.299}$	68.48 ± 1.85
$H(z)$ + BAO + SNP +		$0.0296^{+0.0048}_{-0.0047}$	$0.1067^{+0.0153}_{-0.0154}$	0.286 ± 0.021	$-0.035^{+0.071}_{-0.085}$	$0.550^{+0.231}_{-0.314}$	69.15 ± 2.53

^a w_X corresponds to flat/nonflat XCDM and α corresponds to flat/nonflat ϕ CDM.^b $\text{km s}^{-1} \text{Mpc}^{-1}$.

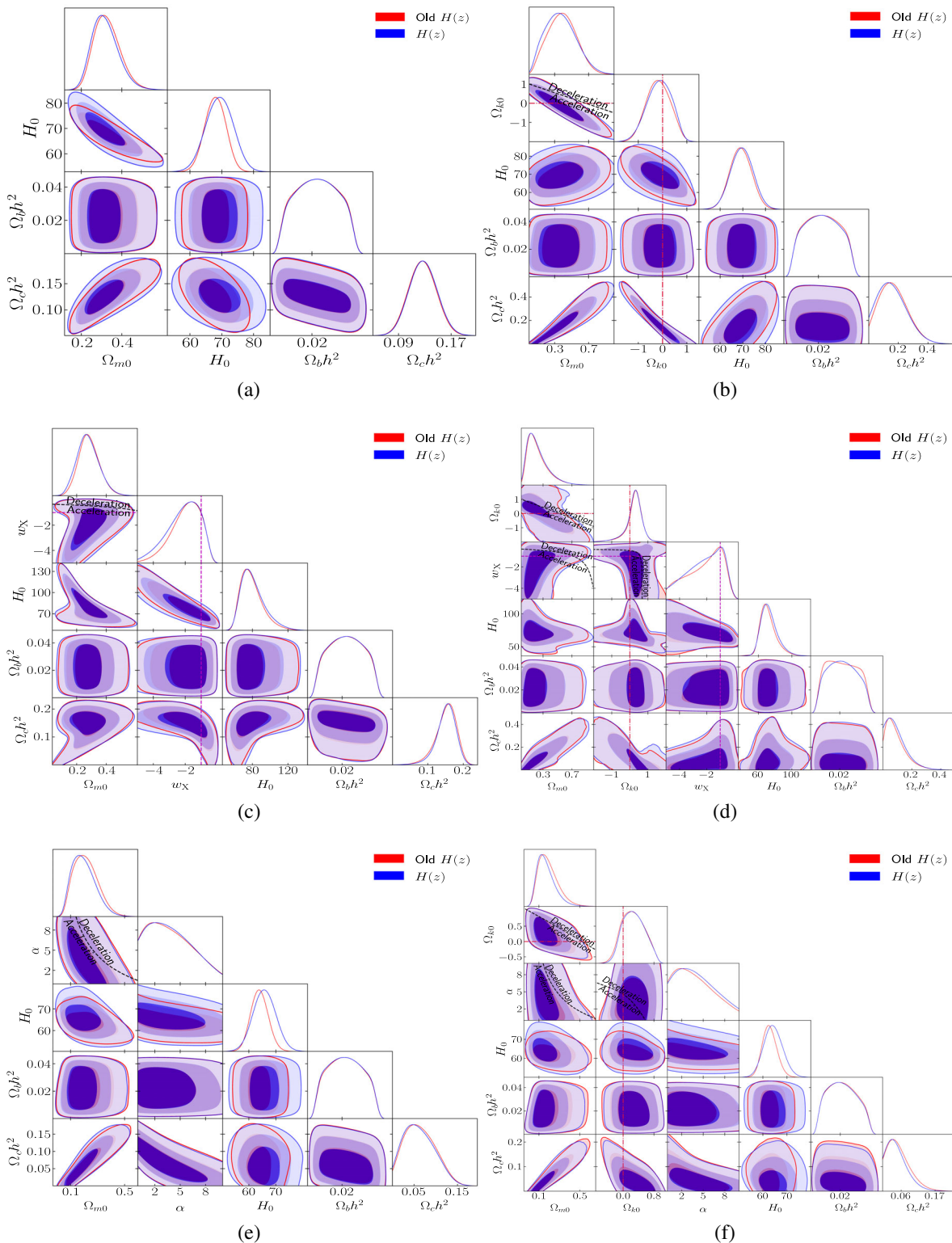


FIG. 1. One-dimensional likelihoods and 1σ , 2σ , and 3σ two-dimensional likelihood confidence contours from old $H(z)$ (red) and $H(z)$ (blue) data for six different models. The black dashed zero-acceleration lines in panels (b)–(f), computed for the third cosmological parameter set to the $H(z)$ +BAO best-fitting values listed in Table IV in panels (d) and (f), divides the parameter space into regions associated with currently accelerating (below or below left) and currently decelerating (above or above right) cosmological expansion. The crimson dash-dot lines represent flat hypersurfaces, with closed spatial hypersurfaces either below or to the left. The magenta lines represent $w_X = -1$, i.e., flat or nonflat Λ CDM models. The $\alpha = 0$ axes correspond to flat and nonflat Λ CDM models in panels (e) and (f), respectively.

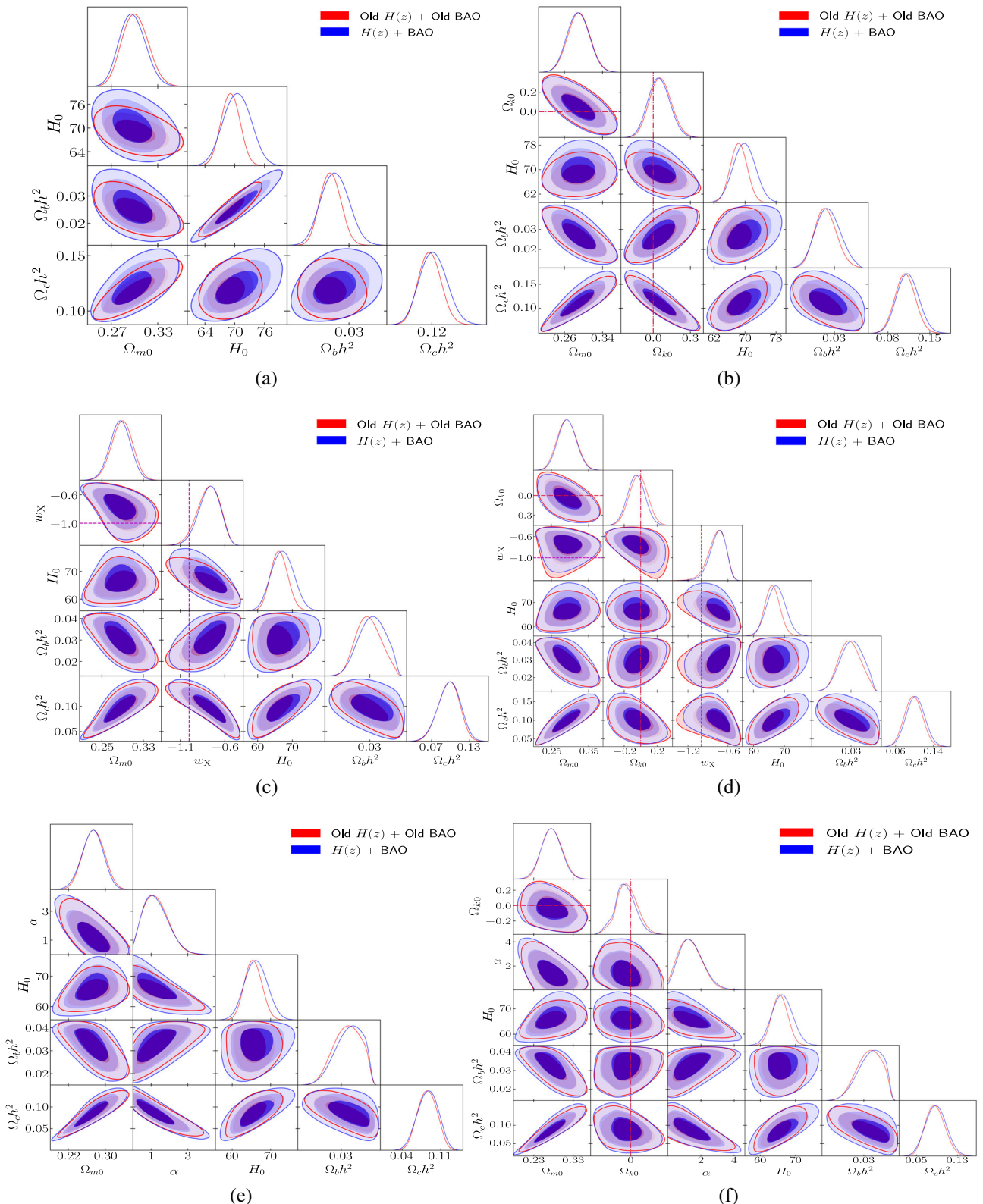


FIG. 2. Same as Fig. 1 but for old $H(z)$ + old BAO (red) and $H(z)$ + BAO (blue) data.

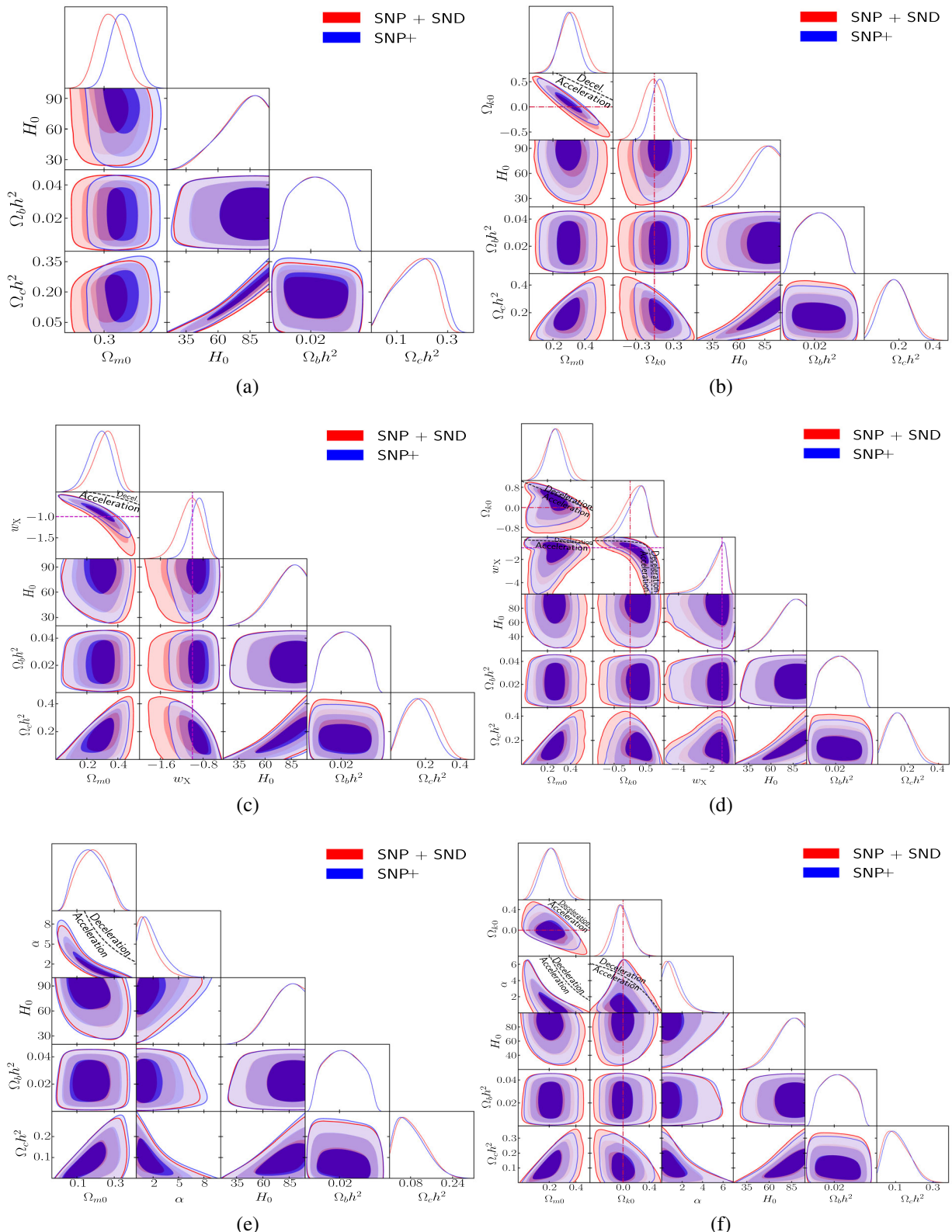


FIG. 3. Same as Fig. 1 but for $\text{SNP} + \text{SND}$ (red) and $\text{SNP}+$ (blue) data. The black dashed zero-acceleration lines in panels (b)–(f), computed for the third cosmological parameter set to the $H(z) + \text{BAO}$ data best-fitting values listed in Table IV in panels (d) and (f), divides the parameter space into regions associated with currently accelerating (below or below left) and currently decelerating (above or above right) cosmological expansion.

favor values of Ω_{m0} lower by $\lesssim 0.17\sigma$ and ranging from $0.272^{+0.024}_{-0.022}$ (flat ϕ CDM) to $0.297^{+0.015}_{-0.017}$ (flat Λ CDM), with a difference of 0.85σ .

Old $H(z)$ + old BAO data constraints on H_0 range from $65.47^{+2.22}_{-2.21}$ $\text{km s}^{-1} \text{Mpc}^{-1}$ (flat ϕ CDM) to 69.14 ± 1.85 $\text{km s}^{-1} \text{Mpc}^{-1}$ (flat Λ CDM), with a difference of 1.3σ . In contrast, $H(z)$ + BAO data favor values of H_0 higher by $\lesssim 0.41\sigma$ (and with larger error bars), ranging from $66.19^{+2.89}_{-2.88}$ $\text{km s}^{-1} \text{Mpc}^{-1}$ (flat ϕ CDM) to 70.49 ± 2.74 $\text{km s}^{-1} \text{Mpc}^{-1}$ (flat Λ CDM), with a difference of 1.1σ .

Old $H(z)$ + old BAO data constraints on Ω_{k0} are $0.059^{+0.081}_{-0.091}$, -0.027 ± 0.109 , and $-0.034^{+0.087}_{-0.098}$ for nonflat Λ CDM, XCDM, and ϕ CDM, respectively. In contrast, $H(z)$ + BAO data constraints on Ω_{k0} are $0.047^{+0.082}_{-0.089}$, -0.054 ± 0.103 , and $-0.052^{+0.093}_{-0.087}$ for nonflat Λ CDM, XCDM, and ϕ CDM, which are 0.10σ , 0.18σ , and 0.13σ lower than those from old $H(z)$ + old BAO data, respectively. In contrast to old $H(z)$ and $H(z)$ data, both old $H(z)$ + old BAO and $H(z)$ + BAO data indicate that open spatial geometry is mildly favored by nonflat Λ CDM, and closed spatial geometry is mildly favored by nonflat XCDM and nonflat ϕ CDM, but flat hypersurfaces are still within 1σ .

Both old $H(z)$ + old BAO data and $H(z)$ + BAO data show strong evidence for dark energy dynamics. In the old $H(z)$ + old BAO data case, for flat (nonflat) XCDM (1σ and 2σ), $w_X = -0.784^{+0.140}_{-0.107}{}^{+0.230}_{-0.243}$ ($w_X = -0.770^{+0.149}_{-0.098}{}^{+0.233}_{-0.256}$), with central values being $< 2\sigma$ higher than $w_X = -1$ (Λ CDM); and for flat (nonflat) ϕ CDM (1σ and 2σ), $\alpha = 1.267^{+0.536}_{-0.807}{}^{+1.240}_{-1.221}$ ($\alpha = 1.360^{+0.584}_{-0.819}{}^{+1.289}_{-1.300}$), with central values being $> 2\sigma$ away from $\alpha = 0$ (Λ CDM). In the $H(z)$ + BAO data case, for flat (nonflat) XCDM (1σ and 2σ), $w_X = -0.776^{+0.130}_{-0.103}{}^{+0.221}_{-0.232}$ ($w_X = -0.757^{+0.135}_{-0.093}{}^{+0.215}_{-0.236}$), with central values being $< 2\sigma$ ($> 2\sigma$) higher than $w_X = -1$ (Λ CDM); and for flat (nonflat) ϕ CDM (1σ and 2σ), $\alpha = 1.271^{+0.507}_{-0.836}{}^{+1.294}_{-1.228}$ ($\alpha = 1.427^{+0.572}_{-0.830}{}^{+1.365}_{-1.317}$), with central values being $> 2\sigma$ away from $\alpha = 0$ (Λ CDM).

Since SN Ia data alone cannot constrain H_0 we choose a narrower prior of $H_0 \in [20, 100]$ $\text{km s}^{-1} \text{Mpc}^{-1}$ for these data. The constraints on H_0 derived from those on $\Omega_b h^2$ and $\Omega_c h^2$ for both SN Ia datasets provide 2σ lower limits that are in agreement with H_0 constraints derived from other data.

SNP + SND data constraints on Ω_{m0} range from $0.181^{+0.075}_{-0.076}$ (flat ϕ CDM) to 0.317 ± 0.068 (nonflat Λ CDM), with a difference of 1.3σ . In contrast, SNP + data constraints on Ω_{m0} differ from the SNP + SND ones by -0.35σ to 0.76σ , ranging from $0.175^{+0.065}_{-0.092}$ (flat ϕ CDM) to 0.332 ± 0.020 (flat Λ CDM), with a difference of 2.3σ .

SNP + SND data constraints on Ω_{k0} are $-0.017^{+0.172}_{-0.174}$, $0.130^{+0.426}_{-0.249}$, and $-0.026^{+0.126}_{-0.150}$ for nonflat Λ CDM, XCDM, and ϕ CDM, respectively. In contrast, SNP+ data

constraints on Ω_{k0} are 0.089 ± 0.132 , $0.215^{+0.350}_{-0.202}$, and $-0.001^{+0.108}_{-0.132}$ for nonflat Λ CDM, XCDM, and ϕ CDM, which are 0.49σ , 0.18σ , and 0.14σ higher than those from SNP + SND data, respectively. SNP + SND data show that open spatial geometry is mildly favored by nonflat XCDM, and closed spatial geometry is mildly favored by nonflat Λ CDM and ϕ CDM; while SNP+ data show that open geometry is mildly favored by nonflat Λ CDM, XCDM, and ϕ CDM. Both sets of data indicate that flat hypersurfaces remain within the 1σ confidence interval, with the exception of the nonflat XCDM scenario, where SNP+ data deviates by 1.1σ from flatness.

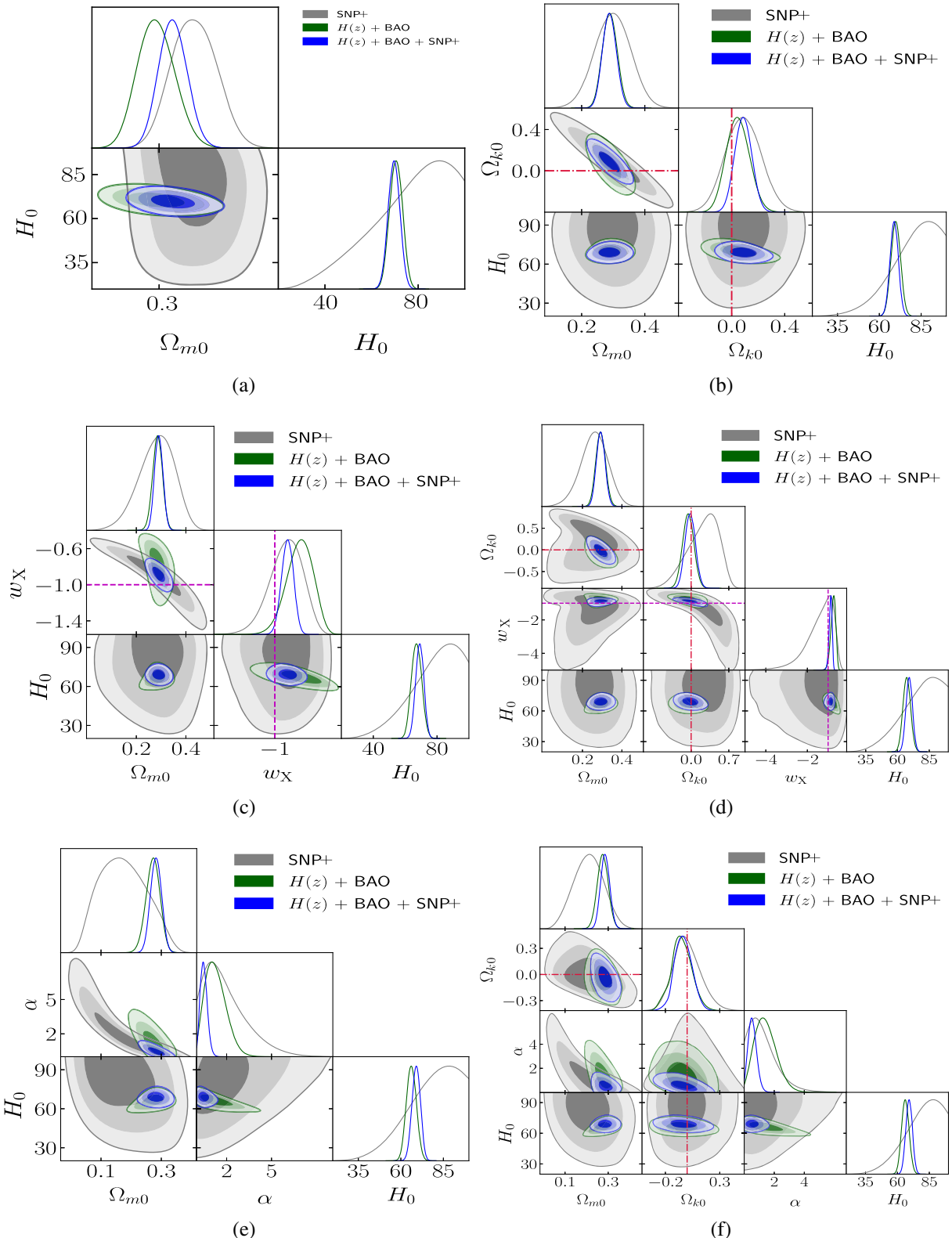
Both SNP + SND and SNP+ data show a slight preference for dark energy dynamics, but deviations from the Λ CDM models are within 1σ . In the SNP + SND case, for flat (nonflat) XCDM, $w_X = -1.054^{+0.237}_{-0.171}$ ($w_X = -1.499^{+0.901}_{-0.237}$), with central values being 0.23σ (0.55σ) lower than $w_X = -1$ (Λ CDM); and for flat (nonflat) ϕ CDM, 2σ upper limits of $\alpha < 4.052$ and $\alpha < 3.067$ suggest that $\alpha = 0$ (Λ CDM) is within 1σ . In the SNP + case, for flat (nonflat) XCDM, $w_X = -0.900^{+0.166}_{-0.124}$ ($w_X = -1.424^{+0.798}_{-0.251}$), with central values being 0.81σ (0.53σ) higher (lower) than $w_X = -1$ (Λ CDM); and for flat (nonflat) ϕ CDM, $\alpha = 1.966^{+0.479}_{-1.907}$ ($\alpha = 1.282^{+0.290}_{-1.255}$), with both central values being 1.0σ away from $\alpha = 0$ (Λ CDM).

B. Constraints from old $H(z)$ + old BAO + SNP + SND data and $H(z)$ + BAO + SNP + data

For old $H(z)$ + old BAO + SNP + SND and $H(z)$ + BAO + SNP+ data, the best-fitting parameter values, likelihood values, and information criteria values for all models are given in Table IV and the marginalized posterior mean parameter values and uncertainties for all models are listed in Table V. Figures 4 and 5 show the probability distributions and confidence regions of cosmological parameters, obtained from SNP+, $H(z)$ + BAO, $H(z)$ + BAO + SNP+, and old $H(z)$ + old BAO + SNP + SND data. Constraints from SNP+, $H(z)$, and BAO data are mutually consistent so these data can be used together to constrain cosmological parameters, as discussed below. Note that the old $H(z)$ + old BAO + SNP + SND data results are from Ref. [58] and are used here to compare to $H(z)$ +BAO + SNP+ constraints.

$H(z)$ +BAO + SNP + (HzBSN) data constraints on Ω_{m0} range from 0.282 ± 0.018 (flat ϕ CDM) to 0.312 ± 0.013 (flat Λ CDM), with a difference of 1.4σ . In contrast, old $H(z)$ + old BAO + SNP + SND data favor values of Ω_{m0} higher by $\lesssim 0.22\sigma$ (or lower by 0.42σ for flat Λ CDM) and ranging from 0.287 ± 0.017 (flat ϕ CDM) to $0.304^{+0.014}_{-0.015}$ (flat Λ CDM), with a difference of 0.75σ .

HzBSN data constraints on H_0 range from 68.89 ± 2.44 $\text{km s}^{-1} \text{Mpc}^{-1}$ (nonflat Λ CDM) to 69.65 ± 2.48 $\text{km s}^{-1} \text{Mpc}^{-1}$ (flat Λ CDM), with a difference of

FIG. 4. Same as Fig. 1 but for SNP+ (gray), $H(z) + \text{BAO}$ (green), and $H(z) + \text{BAO} + \text{SNP+}$ (blue) data.

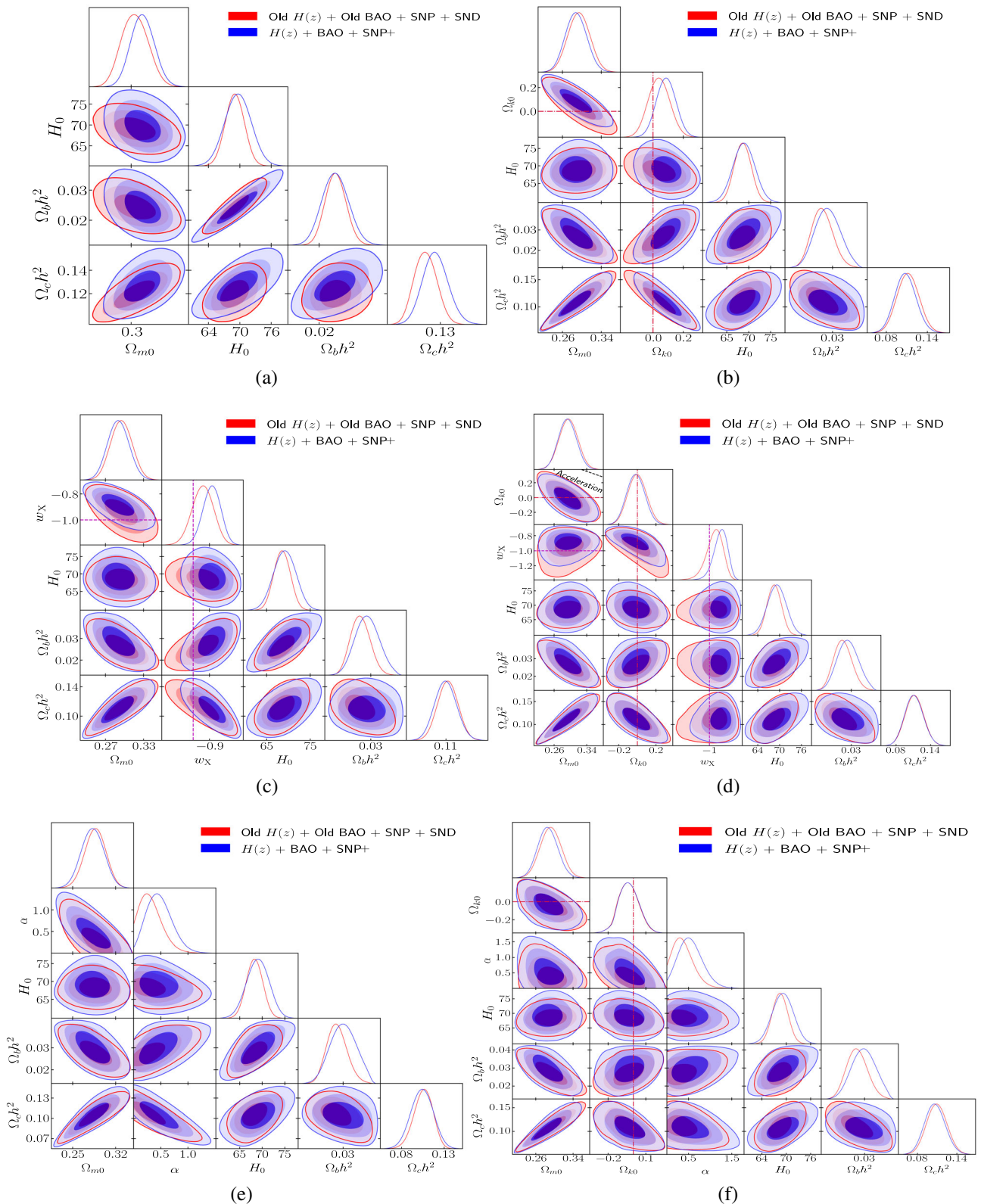


FIG. 5. Same as Fig. 1 but for old $H(z)$ + old BAO + SNP + SND (red) and $H(z)$ + BAO + SNP+ (blue) data.

0.22σ . These H_0 values are 0.24σ (nonflat Λ CDM) and 0.44σ (flat Λ CDM) higher than the median statistics estimate of $H_0 = 68 \pm 2.8 \text{ km s}^{-1} \text{ Mpc}^{-1}$ [59], 0.31σ (nonflat Λ CDM) and 0.05σ (flat Λ CDM) lower than the TRGB and SN Ia estimate of $H_0 = 69.8 \pm 1.7 \text{ km s}^{-1} \text{ Mpc}^{-1}$ [60], and 1.6σ (nonflat Λ CDM) and 1.3σ (flat Λ CDM) lower than the Cepheids and SN Ia measurement of $73.04 \pm 1.04 \text{ km s}^{-1} \text{ Mpc}^{-1}$ [61]. The H_0 constraints from flat Λ CDM is 0.90σ higher than the H_0 estimate of $67.36 \pm 0.54 \text{ km s}^{-1} \text{ Mpc}^{-1}$ from *Planck* 2018 TT, TE, EE + lowE + lensing CMB anisotropy data [7]. In contrast, old $H(z)$ + old BAO + SNP + SND data favor values of H_0 lower by $\lesssim 0.41\sigma$ (and with smaller error bars), ranging from $68.29 \pm 1.78 \text{ km s}^{-1} \text{ Mpc}^{-1}$ (flat ϕ CDM) to $69.04 \pm 1.77 \text{ km s}^{-1} \text{ Mpc}^{-1}$ (flat Λ CDM), with a difference of 0.30σ .

HzBSN data constraints on Ω_{k0} are 0.087 ± 0.063 , -0.017 ± 0.095 , and $-0.035^{+0.071}_{-0.085}$ for nonflat Λ CDM, XCDM, and ϕ CDM, respectively. In contrast, old $H(z)$ + old BAO + SNP + SND data constraints on Ω_{k0} are 0.040 ± 0.070 , -0.001 ± 0.098 , and $-0.038^{+0.071}_{-0.085}$ for nonflat Λ CDM, XCDM, and ϕ CDM, which are 0.50σ lower, 0.12σ higher, and 0.027σ lower than those from HzBSN data, respectively. For both datasets, nonflat Λ CDM favors open spatial geometry, with HzBSN data being 1.4σ away from flat and old $H(z)$ + old BAO + SNP + SND data being within 1σ of flat, while closed spatial geometry is favored by nonflat XCDM and nonflat ϕ CDM, with flatness well within 1σ .

HzBSN data indicate a strong preference for dark energy dynamics. In particular, the central values of the XCDM equation of state parameter, w_X , are found to be $> 2\sigma$ and slightly $< 2\sigma$ higher than -1 for flat and nonflat parametrizations respectively. Similarly, the central values of the parameter α in both the flat and nonflat ϕ CDM models are found to be $> 2\sigma$ away from 0. Note that these constraints are skewed and non-Gaussian. old $H(z)$ + old BAO + SNP + SND data show somewhat less preference for dark energy dynamics. Specifically, for flat (nonflat) XCDM, $w_X = -0.941 \pm 0.064$ ($w_X = -0.948^{+0.098}_{-0.068}$), with central values being 0.92σ (0.76σ) higher than $w_X = -1$, and for flat (nonflat) ϕ CDM, $\alpha = 0.324^{+0.122}_{-0.264}$ ($\alpha = 0.382^{+0.151}_{-0.299}$), with central values being 1.2σ (1.3σ) away from $\alpha = 0$.

Relative to the old $H(z)$ + old BAO + SNP + SND data constraints of Ref. [58], the most significant changes in the constraints from HzBSN data are that they more strongly favor dark energy dynamics and provide larger H_0 error bars.

C. Constraints from QSO-AS + H II G + Mg II + C IV + A118 data

Constraints from QSO-AS + H II G , Mg II + C IV, and A118 data are listed in Tables VI and VII, and their

confidence regions are shown in Fig. 6. Note that A118 results here are corrected with respect to the ones reported in Ref. [42] and used in Ref. [58]. Since the changes are insignificant we do not discuss these results in detail here. QSO-AS + H II G , Mg II + C IV, and A118 data constraints are mutually consistent, so these data can be used together to constrain cosmological parameters, as discussed next.

Joint QSO-AS + H II G + Mg II + C IV + A118 (QHMCA) data constraints on Ω_{m0} range from $0.175^{+0.074}_{-0.080}$ (flat ϕ CDM) to 0.313 ± 0.045 (flat XCDM), with a difference of 1.6σ .

QHMCA data constraints on H_0 range from $70.63 \pm 1.85 \text{ km s}^{-1} \text{ Mpc}^{-1}$ (nonflat ϕ CDM) to $73.51^{+2.15}_{-2.52} \text{ km s}^{-1} \text{ Mpc}^{-1}$ (flat XCDM), with a difference of 0.92σ . These H_0 values are 0.78σ (nonflat ϕ CDM) and 1.5σ (flat XCDM) higher than the median statistics estimate of $H_0 = 68 \pm 2.8 \text{ km s}^{-1} \text{ Mpc}^{-1}$ [59] (also see Refs. [137,138]), 0.33σ (nonflat ϕ CDM) and 1.2σ (flat XCDM) higher than the TRGB and SN Ia estimate of $H_0 = 69.8 \pm 1.7 \text{ km s}^{-1} \text{ Mpc}^{-1}$ [60], and 1.1σ (nonflat ϕ CDM) lower and 0.17σ (flat XCDM) higher than the Cepheids and SN Ia measurement of $73.04 \pm 1.04 \text{ km s}^{-1} \text{ Mpc}^{-1}$ [61]. The H_0 constraints from flat Λ CDM here, $71.43 \pm 1.73 \text{ km s}^{-1} \text{ Mpc}^{-1}$, is 2.2σ higher than the H_0 estimate of $67.36 \pm 0.54 \text{ km s}^{-1} \text{ Mpc}^{-1}$ from *Planck* 2018 TT, TE, EE + lowE + lensing CMB anisotropy data [7].

QHMCA data constraints on Ω_{k0} are $-0.157^{+0.109}_{-0.211}$, $0.039^{+0.219}_{-0.229}$, and $0.018^{+0.083}_{-0.282}$ for nonflat Λ CDM, XCDM, and ϕ CDM, respectively. The nonflat Λ CDM result favors closed spatial geometry, being 1.4σ away from flat, while open spatial geometry is favored in both the nonflat XCDM and nonflat ϕ CDM models, but with flatness well within 1σ .

QHMCA data indicate a preference for dark energy dynamics. In particular, the central values of the XCDM equation of state parameter, w_X , are found to be 1.1σ and 0.83σ lower than -1 for the flat and nonflat parametrizations, respectively. 2σ upper limits of α in both the flat and nonflat ϕ CDM models suggest $\alpha = 0$ is within 1σ .

QSO-AS + H II G + Mg II + C IV + A118 data constraints derived here are very consistent with the QSO-AS + H II G + Mg II + A118 data constraints derived in Ref. [58].

D. Constraints from $H(z)$ + BAO + SNP + + QSO-AS + H II G + Mg II + C IV + A118 and old $H(z)$ + old BAO + SNP + SND + QSO-AS + H II G + Mg II + A118 data

For $H(z)$ +BAO + SNP + + QSO-AS + H II G + Mg II + C IV + A118 (HzBSNQHMCA) data and old $H(z)$ + old BAO + SNP + SND + QSO-AS + H II G + Mg II + A118 (OHZBSNQHMA) data, the best-fitting parameter values, likelihood values, and information criteria values for all models are given in Table VI and the marginalized posterior mean parameter values and uncertainties for all models are

TABLE VI. Unmarginalized best-fitting parameter values for all models from various combinations of data.

Model	Dataset	$\Omega_b h^2$	$\Omega_c h^2$	$\Omega_m \alpha^a$	$\Omega_{\Lambda 0}$	w_X/α^a	H_0^b	l_m	γ_m	β_m	σ_{inflM}	γ_c	β_c	σ_{inflC}	γ_Λ	β_Λ	σ_{inflA}	$-2 \ln \mathcal{L}_{\text{max}}$	AIC	BIC	DIC	ΔAIC	ΔBIC	ΔDIC		
Flat Λ CDM	QSO-AS + H II G	0.0332	0.0947	0.251	71.53	11.06	786.45	794.45	809.28	792.69	0.00	0.00	0.00	0.00	0.00
	Mg II + C IV	...	0.0082	0.068	0.286	1.647	0.280	0.412	0.995	0.274	50.94	64.94	84.21	69.10	0.00	0.00	0.00	0.00	0.00
	A118	...	0.2768	0.616	1.166	49.92	0.382	118.63	126.63	137.71	125.95	0.00	0.00	0.00	0.00	0.00
	QHMCA ^c	0.0376	0.0925	0.256	71.45	11.01	0.286	1.686	0.287	0.435	1.066	0.274	1.205	49.99	0.380	958.61	984.61	1040.28	984.21	0.00	0.00	0.00	0.00	0.00
	H ₂ BSN ^d	0.0239	0.1256	0.312	69.35	1439.59	1445.59	1461.79	1446.05	0.00	0.00	0.00	0.00	0.00
	OHzBSNQHMA ^e	0.0258	0.1207	0.300	70.06	10.93	0.296	1.671	0.286	1.110	50.26	0.406	2031.30	2105.13	2105.18	2051.86	0.00	0.00	0.00	0.00	0.00	
	H ₂ BSNQHMA ^f	0.0258	0.1279	0.309	70.64	10.81	0.306	1.687	0.273	0.423	1.095	0.268	1.219	49.93	0.383	2400.54	2426.54	2500.41	2427.47	0.00	0.00	0.00	0.00	0.00
	H ₂ BSNQMCA ^g	0.0246	0.1291	0.316	69.94	10.88	0.289	1.699	0.273	0.446	1.047	0.287	1.165	50.08	0.380	1964.13	1990.13	2062.86	1990.91	0.00	0.00	0.00	0.00	0.00
Nonflat Λ CDM	QSO-AS + H II G	0.0228	0.1145	0.260	-0.360	...	72.91	11.60	784.18	794.18	812.71	793.24	-0.27	3.43	0.55
	Mg II + C IV	...	0.0791	0.213	-0.678	0.293	1.642	0.279	0.512	1.018	0.269	42.92	58.92	80.95	68.83	-6.01	-3.26	-0.27	
	A118	...	0.4633	0.997	1.553	1.177	49.71	0.380	117.47	127.47	141.32	126.29	0.84	3.61	0.34
	QHMCA ^c	0.0301	0.0997	0.246	-0.229	...	72.83	11.49	0.311	1.668	0.274	0.432	1.042	0.271	1.172	50.10	0.387	957.08	985.08	1045.03	984.54	0.47	4.75	0.33
	H ₂ BSN ^d	0.0276	0.1078	0.288	0.084	...	68.69	1437.61	1445.61	1467.21	1446.04	0.02	5.42	-0.01
	OHzBSNQHMA ^e	0.0261	0.1182	0.297	0.098	...	69.90	10.94	0.301	1.674	0.281	1.126	50.20	0.400	2031.26	2053.26	2112.48	2053.69	1.96	7.35	1.84	
	H ₂ BSNQHMA ^f	0.0296	0.1100	0.286	0.088	...	70.00	10.85	0.311	1.670	0.280	0.444	1.054	0.278	1.234	49.90	0.381	2398.84	2426.84	2506.39	2427.33	0.30	5.98	-0.14
	H ₂ BSNQMCA ^g	0.0268	0.1061	0.289	0.098	...	68.01	11.20	0.292	1.694	0.274	0.430	1.049	0.277	1.167	50.13	0.384	1962.87	1990.87	2069.20	1991.12	0.74	6.34	0.21
Flat XCDM	QSO-AS + H II G	0.0174	0.1308	0.285	...	-1.280	72.32	11.23	786.05	796.05	814.58	795.03	1.60	5.30	2.34
	Mg II + C IV	...	-0.0212	0.008	...	-4.875	...	0.248	1.399	0.262	0.337	0.757	0.225	40.24	56.24	78.27	66.94	-8.70	-5.95	-2.16	
	A118	...	-0.0223	0.006	...	-0.203	1.186	49.87	0.383	118.07	128.07	141.92	126.87	1.44	4.21	0.92
	QHMCA ^c	0.0275	0.1323	0.305	...	-1.607	72.58	11.43	0.288	1.667	0.276	0.438	1.053	0.265	1.176	50.11	0.384	957.29	985.29	1045.24	984.99	0.68	4.96	0.78
	H ₂ BSN ^d	0.0283	0.1092	0.290	...	-0.883	68.96	1434.63	1442.63	1464.22	1443.28	-2.96	2.43	-0.77
	OHzBSNQHMA ^e	0.0266	0.1162	0.296	...	-0.975	69.62	10.94	0.278	1.696	0.280	1.118	50.24	0.406	2030.88	2052.88	2112.10	2053.30	1.58	6.97	1.44	
	H ₂ BSNQHMA ^f	0.0298	0.1056	0.282	...	-0.879	69.45	10.89	0.279	1.708	0.286	0.435	1.068	0.283	1.195	50.01	0.384	2396.06	2424.06	2503.61	2425.97	-2.48	3.20	-1.50
	H ₂ BSNQMCA ^g	0.0288	0.1135	0.296	...	-0.892	69.43	10.80	0.289	1.684	0.287	0.411	1.100	0.287	1.166	50.08	0.381	1960.06	1988.06	2066.39	1988.01	-2.07	3.52	-2.90
Nonflat XCDM	QSO-AS + H II G	0.0300	0.0031	0.065	-0.560	-0.651	71.87	11.45	781.18	793.18	815.43	799.59	-1.27	6.15	6.90
	Mg II + C IV	...	-0.0149	0.021	-0.034	-5.000	...	0.285	1.262	0.270	0.374	0.808	0.226	32.43	50.43	75.21	68.46	-14.51	-9.00	-0.71	
	A118	...	0.4579	0.986	1.260	-1.127	1.179	49.71	0.383	117.50	129.50	146.12	126.97	2.87	8.41	1.02
	QHMCA ^c	0.0248	0.1329	0.293	-0.196	-1.194	73.47	11.37	0.300	1.673	0.278	0.422	1.062	0.289	1.168	50.09	0.394	956.99	986.99	1051.22	986.72	2.38	10.94	2.51
	H ₂ BSN ^d	0.0278	0.1118	0.294	-0.032	-0.865	69.07	1434.46	1444.46	1471.45	1454.42	-1.13	9.66	-0.63
	OHzBSNQHMA ^e	0.0260	0.1158	0.295	-0.016	-0.947	69.53	10.94	0.277	1.697	0.288	1.151	50.15	0.409	2030.78	2054.78	2119.38	2055.42	3.48	14.25	3.56	
	H ₂ BSNQHMA ^f	0.0286	0.1093	0.286	0.007	-0.900	69.87	10.80	0.306	1.692	0.274	0.443	1.062	0.276	1.222	49.93	0.387	2396.10	2426.10	2511.33	2427.35	-0.44	1.09	-0.12
	H ₂ BSNQMCA ^g	0.0288	0.1079	0.287	-0.002	-0.873	69.13	10.83	0.299	1.689	0.283	0.431	1.035	0.273	1.160	50.10	0.384	1959.83	1989.83	2073.76	1989.54	-0.30	10.89	-1.36
Flat ϕ CDM	QSO-AS + H II G	0.0198	0.1066	0.249	...	0.000	71.42	11.10	786.46	796.46	815.00	796.31	2.01	5.72	3.62
	Mg II + C IV	...	-0.0078	0.035	...	0.014	...	0.265	1.662	0.283	0.399	0.984	0.263	51.19	67.19	89.21	72.04	2.25	5.00	2.94	
	A118	...	0.1226	0.301	...	9.805	1.173	49.89	0.383	118.24	128.24	142.10	125.51	1.62	4.39	-0.44
	QHMCA ^c	0.0227	0.1014	0.243	...	0.009	71.72	11.15	0.299	1.685	0.272	0.419	1.070	0.280	1.222	49.97	0.392	958.98	986.98	1046.93	988.57	2.37	6.65	4.36
	H ₂ BSN ^d	0.0288	0.1060	0.286	...	0.402	68.84	1434.43	1442.43	1464.02	1442.92	-3.16	2.23	-3.14
	OHzBSNQHMA ^e	0.0274	0.1116	0.289	...	0.150	69.51	10.97	0.292	1.685	0.280	1.121	50.23	0.409	2030.52	2052.52	2111.74	2053.18	1.22	6.61	1.33	
	H ₂ BSNQHMA ^f	0.0292	0.1152	0.294	...	0.286	70.28	10.78	0.286	1.696	0.286	0.426	1.067	0.294	1.183	50.04	0.384	2396.50	2424.50	2504.05	2424.36	-2.04	3.64	-3.11
	H ₂ BSNQMCA ^g	0.0302	0.1073	0.288	...	0.474	69.31	10.77	0.297	1.691	0.271	0.442	1.056	0.275	1.189	50.01	0.390	1959.57	1987.57	2065.90	1987.57	-2.56	3.04	-3.33

(Table continued)

TABLE VI. (Continued)

Model	Dataset	$\Omega_b h^2$	$\Omega_c h^2$	Ω_{m0}	Ω_{k0}	w_X/α^a	H ₀ ^b	l_m	y_m	β_m	σ_{intM}	y_α	β_α	σ_{intA}	$-2 \ln \mathcal{L}_{\text{max}}$	AIC	BIC	DIC	ΔAIC	ΔBIC	ΔDIC		
Nonflat ϕ CDM	QSO-AS + H _{II} G	0.0338	0.0979	0.251	-0.250	0.000	72.53	11.47	784.61	796.61	818.85	801.32	2.16	9.57	8.63		
Mg II + C IV	...	0.0611	0.176	-0.173	0.115	...	0.289	1.659	0.271	0.421	1.034	0.264	50.74	68.74	93.52	72.86	3.80	9.31	3.76		
A118	...	0.2763	0.615	0.383	6.632	1.180	49.87	0.381	118.00	130.00	146.62	126.28	3.37	8.91	0.33			
QHMCA ^c	0.0321	0.1029	0.259	-0.208	0.101	72.42	11.12	0.304	1.676	0.277	0.451	1.039	0.273	1.155	50.11	0.386	957.66	987.66	1051.89	990.25	3.05	11.61	6.04
HzBSN ^d	0.0282	0.1104	0.291	-0.045	0.480	69.13	1434.23	1444.23	1471.22	1444.26	-1.36	9.43	-1.79		
OHzBSNQHIMA ^e	0.0251	0.1207	0.300	-0.056	0.195	69.84	10.91	0.279	1.699	0.284	1.132	50.19	0.411	2030.76	2054.76	2119.36	2055.13	3.46	14.23	3.28	
HzBSNQHIMCA ^f	0.0313	0.1001	0.275	-0.015	0.545	69.33	10.85	0.287	1.694	0.272	0.424	1.059	0.281	1.197	50.00	0.389	2396.34	2426.34	2511.57	2425.80	-0.20	11.16	-1.66
HzBSNQMQCA ^g	0.0287	0.1113	0.291	-0.018	0.380	69.47	10.86	0.288	1.706	0.283	0.448	1.031	0.287	1.182	50.04	0.389	1959.10	1989.10	2073.03	1989.11	-1.03	10.16	-1.80

^aw_X corresponds to flat/nonflat XCDM and α corresponds to flat/nonflat ϕ CDM.^bkm s⁻¹ Mpc⁻¹.^cQSO-AS + H_{II}G + Mg II + C IV + A118.^dH(z) + BAO + SNP +.^eOld H(z) + old BAO + SNP + SND + QSO-AS + H_{II}G + Mg II + A118.^fH(z) + BAO + SNP + + QSO-AS + H_{II}G + Mg II + C IV + A118.^gH(z) + BAO + SNP + + QSO-AS + Mg II + C IV + A118.TABLE VII. One-dimensional posterior mean parameter values and uncertainties ($\pm 1\sigma$ error bars or 2σ limits) for all models from various combinations of data.

Model	Dataset	$\Omega_b h^2$	$\Omega_c h^2$	Ω_{m0}	Ω_{k0}	w_X/α^a	H ₀ ^b	l_m	y_m	β_m	σ_{intM}	y_α	β_α	σ_{intA}	γ_α	β_c	σ_{intC}	γ_c	β_s	σ_{intA}
Flat Λ CDM	QSO-AS + H _{II} G	0.0225 ± 0.0113	0.1076 ^{+0.0197} _{-0.0224}	0.257 ^{+0.037} _{-0.047}	71.52 ± 1.79	11.04 ± 0.34	
Mg II + C IV	< 0.44 ^f	0.292 ± 0.045	1.691 ± 0.061	0.289 ^{+0.023} _{-0.030}	0.440 ± 0.042	1.030 ± 0.089	0.305 ^{+0.037} _{-0.054}	
A118	0.598 ^{+0.329} _{-0.286}	1.171 ± 0.087	49.93 ± 0.25	0.393 ^{+0.027} _{-0.052}	...	
QHMCA ^d	0.0225 ± 0.0117	0.1090 ^{+0.0193} _{-0.0220}	0.260 ^{+0.036} _{-0.045}	0.312 ± 0.013	0.1267 ^{+0.0080} _{-0.0089}	71.43 ± 1.73	11.03 ± 0.34	0.292 ± 0.043	1.690 ± 0.055	0.288 ^{+0.023} _{-0.038}	0.439 ± 0.038	1.030 ^{+0.032} _{-0.053}	0.301 ^{+0.035} _{-0.052}	1.197 ± 0.086	50.02 ± 0.24	0.393 ^{+0.025} _{-0.051}		
HzBSN ^e	0.0243 ± 0.0034	0.1201 ± 0.0020	0.1201 ± 0.0012	0.312 ± 0.013	69.65 ± 2.48	1.131 ± 0.087	50.20 ± 0.24	0.413 ^{+0.026} _{-0.053}	...	
OHzBSNQHIMA ^f	0.0256 ± 0.0020	0.1201 ± 0.0012	0.300 ± 0.012	0.300 ± 0.012	69.87 ± 1.13	10.96 ± 0.25	0.293 ± 0.044	1.684 ± 0.055	0.292 ^{+0.023} _{-0.039}	0.442 ± 0.039	1.035 ^{+0.072} _{-0.063}	0.302 ^{+0.035} _{-0.052}	1.190 ± 0.085	50.02 ± 0.24	0.392 ^{+0.025} _{-0.051}			
HzBSNQHIMCA ^g	0.0250 ± 0.0021	0.1200 ± 0.0012	0.308 ± 0.012	0.313 ± 0.012	69.50 ^{+2.45} _{-2.44}	10.94 ^{+0.39} _{-0.44}	0.294 ± 0.044	1.689 ± 0.055	0.288 ^{+0.023} _{-0.039}	0.442 ± 0.039	1.032 ^{+0.075} _{-0.064}	0.302 ^{+0.035} _{-0.052}	1.190 ± 0.085	50.03 ± 0.24	0.392 ^{+0.025} _{-0.051}			
HzBSNQMQCA ^h	0.0241 ^{+0.0032} _{-0.0035}	0.1263 ^{+0.0080} _{-0.0089}	0.313 ± 0.012	0.313 ± 0.012	72.25 ± 1.99	11.35 ± 0.49	
Nonflat Λ CDM	QSO-AS + H _{II} G	0.0224 ± 0.0111	0.1122 ^{+0.0223} _{-0.0218}	0.260 ^{+0.039} _{-0.045}	-0.196 ^{+0.112} _{-0.205}	0.314 ^{+0.048} _{-0.052}	1.662 ± 0.065	0.285 ^{+0.023} _{-0.030}	0.491 ^{+0.050} _{-0.064}	1.073 ^{+0.033} _{-0.044}	0.299 ^{+0.036} _{-0.053}		
Mg II + C IV	0.473 ^{+0.187} _{-0.311}	-0.818 ^{+0.391} _{-0.637}	1.186 ± 0.087	49.82 ± 0.26	0.392 ^{+0.026} _{-0.051}	...		
A118	> 0.267	0.789 ^{+0.664} _{-0.775}	71.97 ± 1.85	11.24 ± 0.41	0.292 ± 0.043	1.684 ± 0.055	0.288 ^{+0.023} _{-0.038}	0.441 ± 0.038	1.028 ^{+0.031} _{-0.054}	1.298 ^{+0.035} _{-0.052}	1.182 ± 0.087	50.06 ± 0.24	0.395 ^{+0.026} _{-0.051}	...			
QHMCA ^d	0.0224 ± 0.0117	0.1144 ^{+0.0213} _{-0.0212}	0.266 ^{+0.036} _{-0.044}	-0.157 ^{+0.179} _{-0.121}	0.882 ± 0.244	1.131 ± 0.086	50.20 ± 0.24	0.413 ^{+0.027} _{-0.053}	...		
HzBSN ^e	0.0282 ^{+0.0046} _{-0.0050}	0.1082 ± 0.0152	0.288 ± 0.021	0.087 ± 0.053	69.79 ± 1.14	10.96 ± 0.25	0.293 ± 0.044	1.685 ± 0.055	0.292 ^{+0.023} _{-0.039}	0.440 ± 0.038	1.033 ^{+0.073} _{-0.062}	0.303 ^{+0.035} _{-0.052}	1.197 ^{+0.084} _{-0.085}	50.01 ± 0.24	0.392 ^{+0.025} _{-0.051}			
OHzBSNQHIMA ^f	0.0265 ^{+0.0032} _{-0.0038}	0.1168 ± 0.0127	0.295 ± 0.019	0.018 ± 0.056	70.02 ± 1.25	10.87 ± 0.26	0.293 ± 0.044	1.692 ± 0.054	0.288 ^{+0.023} _{-0.039}	0.441 ± 0.039	1.027 ^{+0.075} _{-0.065}	0.303 ^{+0.035} _{-0.052}	1.195 ± 0.085	50.03 ± 0.24	0.392 ^{+0.025} _{-0.051}			
HzBSNQHIMCA ^g	0.0291 ^{+0.0036} _{-0.0041}	0.1115 ± 0.0126	0.288 ± 0.019	0.074 ± 0.056	68.88 ± 2.45	11.04 ^{+0.39} _{-0.35}	0.294 ± 0.044	1.687 ± 0.055	0.288 ^{+0.023} _{-0.039}	0.441 ± 0.039	1.027 ^{+0.075} _{-0.065}	0.303 ^{+0.035} _{-0.052}	1.195 ± 0.085	50.03 ± 0.24	0.392 ^{+0.025} _{-0.051}			
HzBSNQMQCA ^h	0.0273 ^{+0.0041} _{-0.0047}	0.1112 ^{+0.0138} _{-0.0151}	0.293 ± 0.020	0.073 ± 0.059	

(Table continued)

TABLE VII. (*Continued*)

Model	Dataset	$\Omega_b h^2$	$\Omega_c h^2$	Ω_m	Ω_{m0}	Ω_{k0}	w_X/α^a	H_0^b	l_m	γ_m	β_m	$\sigma_{\text{int},M}$	γ_c	β_c	$\sigma_{\text{int},C}$	γ_A	β_A	$\sigma_{\text{int},A}$		
Fiat XCDM	QSO-AS + HII G	0.0224 ± 0.0112	0.1391 ± 0.0333 -0.0256	0.305 ± 0.056 -0.0447	< 0.563	...	-1.683 ± 0.712 -0.387	72.92 ± 2.15 -2.40	11.31 ± 0.43		
Mg II + C IV	0.535 ± 0.277 -0.274	...	-2.521 ± 2.310 -2.310	0.282 ± 0.082 -0.086	1.557 ± 0.117 -0.101	0.405 ± 0.047	0.900 ± 0.122 -0.121	0.282 ± 0.038 -0.034		
A118	0.313 ± 0.045 -0.042	...	-1.929 ± 0.835 -0.426	73.51 ± 2.15 -2.52	11.41 ± 0.43	0.295 ± 0.044	1.677 ± 0.056	0.287 ± 0.023 -0.023	1.029 ± 0.071 -0.064	0.297 ± 0.035 -0.032	1.167 ± 0.088	50.01 ± 0.121 -0.111	0.393 ± 0.026 -0.025	
QHMCA ^d	0.0225 ± 0.0117	0.1457 ± 0.0291 -0.0242	0.313 ± 0.045 -0.042	...	-0.886 ± 0.053 -0.056	69.15 ± 2.52		
H ₂ BSN ^e	0.0287 ± 0.0044	0.1097 ± 0.0117 -0.0116	0.294 ± 0.015 -0.009	...	-0.959 ± 0.059 -0.051	69.66 ± 1.16	10.94 ± 0.25	0.293 ± 0.044	1.685 ± 0.055	0.292 ± 0.023 -0.023	1.034 ± 0.074 -0.062	0.303 ± 0.035 -0.033	1.131 ± 0.087	50.20 ± 0.24	0.413 ± 0.023 -0.023	
OH ₂ BSNQHMCA ^f	0.0271 ± 0.0037	0.1147 ± 0.0098 -0.0097	0.288 ± 0.015 -0.0100	...	-0.895 ± 0.051 -0.050	69.84 ± 1.26	10.80 ± 0.26	0.294 ± 0.044	1.692 ± 0.054	0.288 ± 0.022 -0.022	1.042 ± 0.039	0.303 ± 0.035 -0.033	1.193 ± 0.085	50.01 ± 0.24	0.392 ± 0.025 -0.025	
H ₂ BSNQHMCA ^g	0.0294 ± 0.0040	0.1106 ± 0.0100 -0.0092	0.298 ± 0.015 -0.0145	...	-0.889 ± 0.052 -0.051	69.05 ± 2.40	10.90 ± 0.38	0.294 ± 0.044	1.690 ± 0.055	0.288 ± 0.023 -0.023	1.031 ± 0.075	0.303 ± 0.035 -0.033	1.192 ± 0.084	50.02 ± 0.24	0.392 ± 0.025 -0.025	
H ₂ BSNQMC ^h	0.0284 ± 0.0040	0.1101 ± 0.0112 -0.0105	0.292 ± 0.016 -0.0145	...	-0.889 ± 0.052 -0.051	69.05 ± 2.40	10.90 ± 0.43	0.294 ± 0.044	1.690 ± 0.055	0.288 ± 0.023 -0.023	1.031 ± 0.074	0.303 ± 0.035 -0.033	1.192 ± 0.084	50.02 ± 0.24	0.392 ± 0.025 -0.025	
Nonflat XCDM	QSO-AS + HII G	0.0224 ± 0.0114	0.1122 ± 0.0473 -0.0326	0.258 ± 0.086 -0.057	0.018 ± 0.345 -0.388	-1.670 ± 1.063 -1.245	72.34 ± 2.16	11.20 ± 0.49		
Mg II + C IV	0.338 ± 0.100 -0.099	-0.410 ± 0.368 -0.322	< 1.24	...	0.319 ± 0.048 -0.034	1.526 ± 0.132 -0.108	0.280 ± 0.023 -0.023	0.456 ± 0.047 -0.056	0.966 ± 0.119 -0.110	0.282 ± 0.037 -0.033	1.185 ± 0.090	49.82 ± 0.28	0.392 ± 0.026 -0.026			
A118	> 0.226	0.690 ± 0.512 -0.506	-2.342 ± 2.067 -1.006		
QHMCA ^d	0.0226 ± 0.0118	0.1327 ± 0.0335 -0.0277	0.291 ± 0.056 -0.049	0.039 ± 0.219 -0.229	-2.066 ± 2.87 -0.446	73.13 ± 2.46	11.30 ± 0.46	0.294 ± 0.044	1.680 ± 0.056	0.287 ± 0.023 -0.023	1.439 ± 0.038	1.030 ± 0.065	0.298 ± 0.035	1.187 ± 0.087	50.06 ± 0.24	0.393 ± 0.025 -0.025		
H ₂ BSN ^e	0.0284 ± 0.0047	0.1115 ± 0.0151 -0.0151	0.293 ± 0.021 -0.021	-0.017 ± 0.095 -0.082	-0.884 ± 0.058 -0.058	69.23 ± 2.53		
OH ₂ BSNQHMCA ^f	0.0269 ± 0.0033	0.1155 ± 0.0128 -0.0127	0.295 ± 0.019 -0.019	-0.009 ± 0.077 -0.083	-0.959 ± 0.060 -0.063	69.65 ± 1.16	10.93 ± 0.26	0.293 ± 0.044	1.685 ± 0.055	0.292 ± 0.023 -0.023	1.034 ± 0.074	0.303 ± 0.035	1.192 ± 0.085	50.01 ± 0.24	0.392 ± 0.025 -0.025			
H ₂ BSNQHMCA ^g	0.0293 ± 0.0040	0.1108 ± 0.0124 -0.0124	0.289 ± 0.019 -0.019	-0.004 ± 0.078 -0.078	-0.897 ± 0.055 -0.056	69.81 ± 1.26	10.80 ± 0.27	0.294 ± 0.044	1.692 ± 0.054	0.288 ± 0.022 -0.022	1.442 ± 0.039	1.032 ± 0.064	0.298 ± 0.036	1.189 ± 0.085	50.02 ± 0.24	0.392 ± 0.025 -0.025		
H ₂ BSNQMC ^h	0.0279 ± 0.0042	0.1134 ± 0.0139 -0.0133	0.296 ± 0.020 -0.020	-0.032 ± 0.085 -0.085	-0.877 ± 0.055 -0.053	69.26 ± 2.45	10.84 ± 0.41	0.294 ± 0.043	1.691 ± 0.055	0.289 ± 0.023 -0.023	1.443 ± 0.039	1.032 ± 0.064	0.298 ± 0.036	1.190 ± 0.085	50.02 ± 0.24	0.392 ± 0.025 -0.025		
Flat ϕ CDM	QSO-AS + HII G	0.0217 ± 0.0081	0.0543 ± 0.0225 -0.0211	0.154 ± 0.053 -0.0471	< 0.537	...	< 6.506	70.64 ± 1.80	10.81 ± 0.34		
Mg II + C IV	0.535 ± 0.239 -0.237	0.667 ± 0.393 -0.393	< 6.202 ^c	...	0.299 ± 0.046	1.717 ± 0.039	0.289 ± 0.023 -0.023	0.449 ± 0.043	1.069 ± 0.091 -0.074	0.312 ± 0.037 -0.034	1.171 ± 0.088	49.88 ± 0.24	0.392 ± 0.026 -0.026	
A118	0.535 ± 0.239 -0.237	0.667 ± 0.393 -0.393		
QHMCA ^d	0.0219 ± 0.0082	0.0647 ± 0.0378 -0.0408	0.1175 ± 0.074 -0.080	0.040 ± 0.282 -0.282	0.040 ± 0.198 -0.198	0.475 ± 0.189 -0.265	69.01 ± 2.43		
H ₂ BSN ^e	0.0300 ± 0.0047	0.1040 ± 0.0129	0.282 ± 0.018 -0.018	0.286 ± 0.015 -0.015	0.1089 ± 0.0083 -0.0083	0.249 ± 0.069 -0.069	69.50 ± 1.14	10.92 ± 0.25	0.293 ± 0.044	1.695 ± 0.054	0.292 ± 0.023 -0.023	1.439 ± 0.039	1.033 ± 0.064	0.303 ± 0.035	1.204 ± 0.086	50.00 ± 0.24	0.393 ± 0.025 -0.025	
OH ₂ BSNQHMCA ^f	0.0286 ± 0.0025	0.1089 ± 0.0083	0.286 ± 0.015 -0.015	0.1057 ± 0.0108 -0.0108	0.1057 ± 0.0107 -0.0107	0.423 ± 0.268 -0.268	69.79 ± 1.25	10.79 ± 0.26	0.294 ± 0.044	1.692 ± 0.054	0.288 ± 0.022 -0.022	1.442 ± 0.039	1.034 ± 0.075	0.303 ± 0.035	1.193 ± 0.085	50.01 ± 0.24	0.392 ± 0.025 -0.025	
H ₂ BSNQHMCA ^g	0.0307 ± 0.0038	0.1048 ± 0.0122	0.284 ± 0.017 -0.017	0.1048 ± 0.0102 -0.0102	0.1048 ± 0.0102 -0.0102	0.450 ± 0.253 -0.253	68.92 ± 2.35	10.90 ± 0.37	0.294 ± 0.043	1.690 ± 0.055	0.288 ± 0.023 -0.023	1.442 ± 0.039	1.031 ± 0.064	0.303 ± 0.035	1.192 ± 0.085	50.02 ± 0.24	0.392 ± 0.025 -0.025	
H ₂ BSNQMC ^h	0.0296 ± 0.0043	0.1048 ± 0.0122	0.284 ± 0.017 -0.017	0.1048 ± 0.0102 -0.0102	0.1048 ± 0.0102 -0.0102	0.450 ± 0.253 -0.253	78.75	70.21 ± 1.83	10.70 ± 0.36		
Nonflat ϕ CDM	QSO-AS + HII G	0.0219 ± 0.0081	0.0576 ± 0.0268 -0.0260	0.163 ± 0.058 -0.0434	0.181 ± 0.180 -0.088	< 0.536	0.088 ± 0.384 -0.364	< 1.612 ^c	...	0.299 ± 0.046	1.719 ± 0.055	0.290 ± 0.023 -0.023	0.450 ± 0.043	1.072 ± 0.088 -0.076	0.312 ± 0.037 -0.034	1.174 ± 0.088	49.88 ± 0.24	0.392 ± 0.026 -0.026
Mg II + C IV	0.516 ± 0.215 -0.215	0.664 ± 0.293 -0.293	5.209 ± 3.855 -3.462		
A118	0.516 ± 0.215 -0.215	0.664 ± 0.293 -0.293	5.209 ± 3.855 -3.462		
QHMCA ^d	0.0221 ± 0.0017	0.0742 ± 0.0405 -0.0329	0.194 ± 0.077 -0.063	0.018 ± 0.083 -0.083	0.018 ± 0.077 -0.077	0.1868 ± 0.232 -0.232	< 6.688	70.63 ± 1.85	10.84 ± 0.39	0.292 ± 0.044	1.694 ± 0.055	0.288 ± 0.023 -0.023	1.439 ± 0.039	1.033 ± 0.075	0.303 ± 0.035	1.201 ± 0.086	50.00 ± 0.24	0.393 ± 0.026 -0.026
H ₂ BSN ^e	0.0296 ± 0.0047	0.1067 ± 0.0353 -0.034	0.286 ± 0.021 -0.021	-0.035 ± 0.071 -0.071	0.550 ± 0.231 -0.231	69.15 ± 2.53		
OH ₂ BSNQHMCA ^f	0.0277 ± 0.0034	0.1126 ± 0.0128	0.291 ± 0.019 -0.019	-0.040 ± 0.064 -0.062	0.316 ± 0.101 -0.101	69.52 ± 1.15	10.89 ± 0.25	0.294 ± 0.044	1.685 ± 0.055	0.292 ± 0.023 -0.023	1.439 ± 0.039	1.033 ± 0.074	0.303 ± 0.035	1.203 ± 0.086	50.01 ± 0.24	0.392 ± 0.026 -0.026		
H ₂ BSNQHMCA ^g	0.0303 ± 0.0043	0.1068 ± 0.0127	0.283 ± 0.019 -0.019	-0.021 ± 0.074 -0.074	0.468 ± 0.200 -0.200	69.76 ± 1.25	10.78 ± 0.26	0.294 ± 0.044	1.692 ± 0.054	0.288 ± 0.023 -0.023	1.442 ± 0.039	1.034 ± 0.075	0.303 ± 0.035	1.191 ± 0.084	50.01 ± 0.24	0.392 ± 0.026 -0.026		
H ₂ BSNQMC ^h	0.0292 ± 0.0045	0.1083 ± 0.0144 -0.0145	0.288 ± 0.020 -0.020	-0.044 ± 0.067 -0.067	0.543 ± 0.226 -0.226	69.18 ± 2.43	10.83 ± 0.40	0.294 ± 0.044	1.691 ± 0.055	0.288 ± 0.023 -0.023	1.443 ± 0.039	1.033 ± 0.075	0.303 ± 0.035	1.189 ± 0.085	50.02 ± 0.24	0.392 ± 0.026 -0.026		

^a w_X corresponds to flat/nonflat XCDM and α corresponds to flat/nonflat ϕ CDM.

^b $\text{km s}^{-1} \text{Mpc}^{-1}$.

^cThis is the 1 σ limit. The 2 σ limit is set by the prior and is not shown here.

^dQSO-AS + HII G + Mg II + C IV + A118.

^e $H(z) + \text{BAO} + \text{SNP}^+$.

^fOld $H(z) + \text{BAO} + \text{SNP} + \text{QSO-AS} + \text{HII G} + \text{Mg II} + \text{C IV} + \text{A118}.$

^g $H(z) + \text{BAO} + \text{SNP} + \text{QSO-AS} + \text{HII G} + \text{Mg II} + \text{C IV} + \text{A118}.$

^h $H(z) + \text{BAO} + \text{SNP} + \text{QSO-AS} + \text{HII G} + \text{Mg II} + \text{C IV} + \text{A118}.$

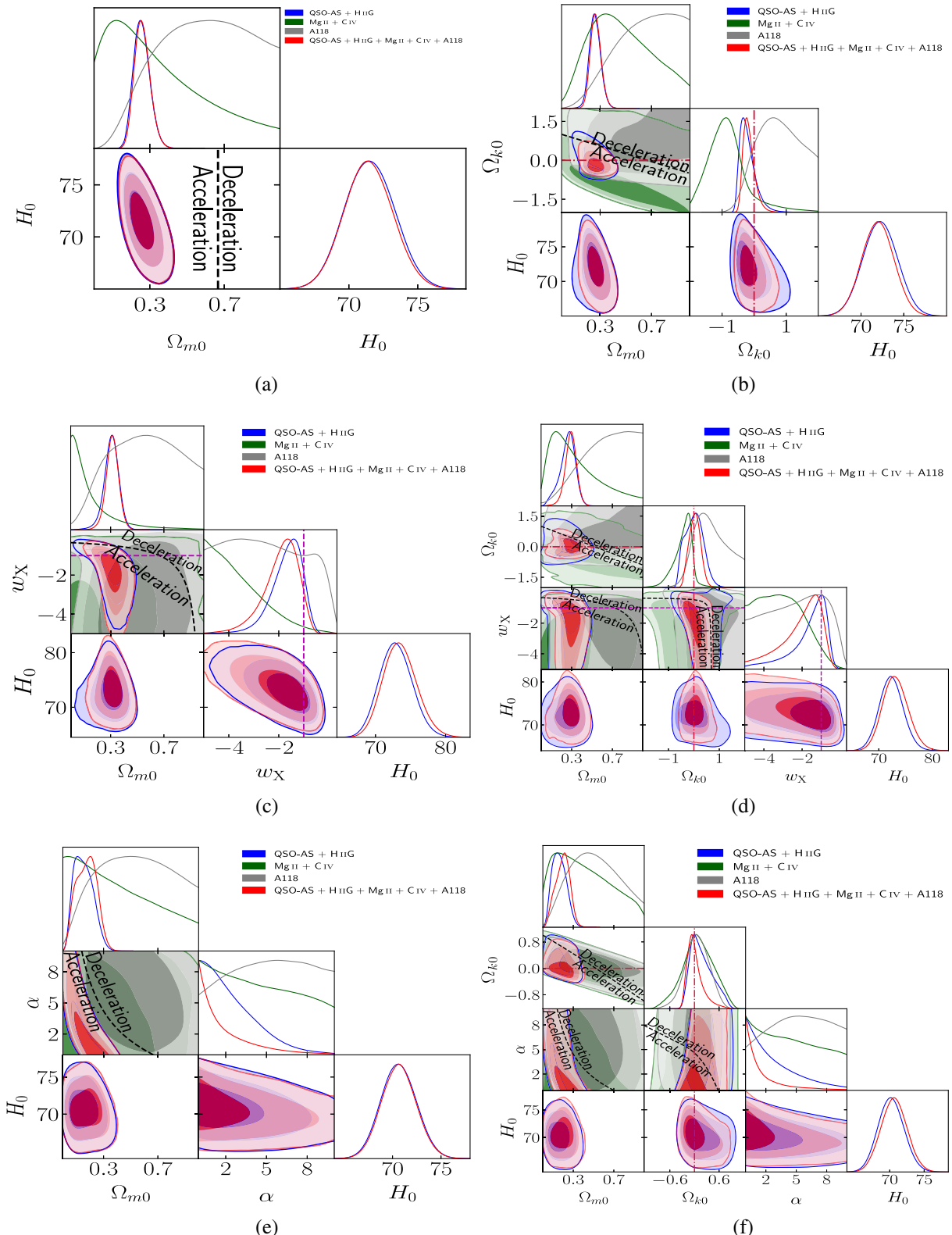


FIG. 6. Same as Fig. 1 but for QSO-AS + H II G (blue), Mg II + C IV (green), A118 (gray), and QSO-AS + H II G + Mg II + C IV + A118 (red) data. The black dashed zero-acceleration lines, computed for the third cosmological parameter set to the $H(z)$ +BAO data best-fitting values listed in Table IV in panels (d) and (f), divides the parameter space into regions associated with currently accelerating (below left) and currently decelerating (above right) cosmological expansion.

listed in Table VII. The OHzBSNQHMA data results are from Ref. [58] and are used here to compare to HzBSNQHMCA data constraints. Note that there is a typo in Table 5 of Ref. [58], where in the flat XCDM OHzBSNQHMA case, $\Omega_b h^2$ should be $0.1147^{+0.0098}_{-0.0097}$ instead of $0.1449^{+0.0098}_{-0.0097}$. Constraints derived without using H II G data are discussed in the Appendix.

Figures 7 and 8 show that $H(z) + \text{BAO} + \text{SNP} +$ and QSO-AS + H II G + Mg II + C IV + A118 data constraints are mutually consistent so these data can be used together to more restrictively constrain cosmological parameter values. Figure 9 compares the probability distributions and confidence regions of cosmological parameters, obtained from HzBSNQHMCA and OHzBSNQHMA data.

HzBSNQHMCA data constraints on Ω_m range from 0.281 ± 0.017 (flat ϕ CDM) to 0.308 ± 0.012 (flat Λ CDM), with a difference of 1.3σ . This difference is somewhat larger than the 0.73σ difference for the OHzBSNQHMA dataset, [58].

HzBSNQHMCA data constraints on $\Omega_b h^2$ range from 0.0250 ± 0.0021 (flat Λ CDM) to $0.0307^{+0.0032}_{-0.0038}$ (flat ϕ CDM), with a difference of 1.3σ . The constraints on $\Omega_c h^2$ range from $0.1057^{+0.0118}_{-0.0107}$ (flat ϕ CDM) to 0.1260 ± 0.0064 (flat Λ CDM), with a difference of 1.5σ .

HzBSNQHMCA data constraints on H_0 range from $69.76 \pm 1.25 \text{ km s}^{-1} \text{ Mpc}^{-1}$ (nonflat ϕ CDM) to $70.13 \pm 1.25 \text{ km s}^{-1} \text{ Mpc}^{-1}$ (flat Λ CDM), with a difference of 0.21σ . This difference is slightly smaller than the 0.23σ difference for the OHzBSNQHMA dataset, [58]. These H_0 values are 0.57σ (nonflat ϕ CDM) and 0.69σ (flat Λ CDM) higher than the median statistics estimate of $H_0 = 68 \pm 2.8 \text{ km s}^{-1} \text{ Mpc}^{-1}$ [59], 0.02σ (nonflat ϕ CDM) lower and 0.16σ (flat Λ CDM) higher than the TRGB and SN Ia estimate of $H_0 = 69.8 \pm 1.7 \text{ km s}^{-1} \text{ Mpc}^{-1}$ [60], and 2.0σ (nonflat ϕ CDM) and 1.8σ (flat Λ CDM) lower than the Cepheids and SN Ia measurement of $73.04 \pm 1.04 \text{ km s}^{-1} \text{ Mpc}^{-1}$ [61]. The H_0 constraints from flat Λ CDM is 2.0σ higher than the H_0 estimate of $67.36 \pm 0.54 \text{ km s}^{-1} \text{ Mpc}^{-1}$ from Planck 2018 TT, TE, EE + lowE + lensing CMB anisotropy data [7].

HzBSNQHMCA data constraints on Ω_{k0} are 0.074 ± 0.056 , -0.004 ± 0.078 , and $-0.021^{+0.067}_{-0.074}$ for nonflat Λ CDM, XCDM, and ϕ CDM, respectively. Nonflat Λ CDM favors open spatial geometry, being 1.3σ away from flat, while closed spatial geometry is favored by nonflat XCDM and nonflat ϕ CDM, with flatness within 1σ . It is interesting that for the non-CMB data compilation of Ref. [81] the two nonflat Λ CDM models, with two different primordial power spectra, favor closed geometry at $\sim 0.7\sigma$, but that non-CMB data compilation includes growth factor measurements and so those constraints also depend on the primordial power spectrum assumed, unlike the constraints we derive here.

HzBSNQHMCA data indicate a strong preference for dark energy dynamics. For flat (nonflat) XCDM (1σ and

2σ), $w_X = -0.895 \pm 0.051^{+0.099}_{-0.105}$ ($w_X = -0.897^{+0.075}_{-0.055}{}^{+0.127}_{-0.139}$), with central values being 2.0σ (1.6σ) higher than $w_X = -1$ (Λ CDM). For flat (nonflat) ϕ CDM (1σ and 2σ), $\alpha = 0.423^{+0.168}_{-0.246}{}^{+0.405}_{-0.393}$ ($\alpha = 0.468^{+0.200}_{-0.292}{}^{+0.454}_{-0.454}$), with central values being $> 2\sigma$ (1.6σ) away from $\alpha = 0$ (Λ CDM).

HzBSNQHMCA data constraints are in good agreement with OHzBSNQHMA data constraints. Specifically, the $\Omega_b h^2$ constraints from the former are between 0.21σ lower (flat Λ CDM) and 0.52σ higher (flat XCDM); the $\Omega_c h^2$ constraints from the former are between 0.32σ lower (nonflat ϕ CDM) and 0.67σ higher (flat Λ CDM); the Ω_{m0} constraints from the former are between 0.30σ lower (nonflat ϕ CDM) and 0.47σ higher (flat Λ CDM); and the H_0 constraints from the former are between 0.093σ higher (nonflat XCDM) and 0.17σ higher (flat ϕ CDM).

In nonflat Λ CDM, XCDM, and ϕ CDM, the Ω_{k0} constraints from HzBSNQHMCA data are 0.69σ , 0.046σ , and 0.19σ higher than those from OHzBSNQHMA data, respectively. In both datasets, open spatial geometry is favored by nonflat Λ CDM, and closed spatial geometry is favored by nonflat XCDM and nonflat ϕ CDM.

In flat and nonflat XCDM and ϕ CDM, the w_X and α constraints from HzBSNQHMCA data are 0.82σ , 0.59σ , 0.68σ , and 0.49σ higher than those from OHzBSNQHMA data, respectively. The former, new, data indicate stronger evidence for dark energy dynamics than do the latter, old data of Ref. [58].

Overall, the changes in constraints found here, using updated and more data and improved analyses, compared to those found in Ref. [58], are not large. This lends hope to the belief that the constraints we have derived here are more than somewhat reliable. We note however some trends from the above numerical values of the differences, and from Fig. 9: in all six models the new HzBSNQHMCA data results here favor slightly larger values of H_0 ; in the four dynamical dark energy models, they favor slightly more dark energy dynamics; and in five of the six models, they favor slightly larger $\Omega_b h^2$ and slightly smaller $\Omega_c h^2$ and Ω_{m0} values, with the exception being the opposite behavior of the flat Λ CDM model.

E. Model comparison

From the AIC, BIC, and DIC values listed in Tables IV and VI, we find the following results:

- (i) **AIC.** Flat Λ CDM is favored the most by $H(z)$, SNP+, A118, and QHMCA data; flat ϕ CDM is favored the most by $H(z) + \text{BAO}$ and $H(z) + \text{BAO} + \text{SNP} +$ data; nonflat XCDM is favored the most by QSO-AS + H II G and Mg II + C IV data; and nonflat XCDM is favored the most by HzBSNQHMCA data.

The evidence against the rest of the models/parametrizations is either only weak or positive, except for the Mg II + C IV data, where the evidence

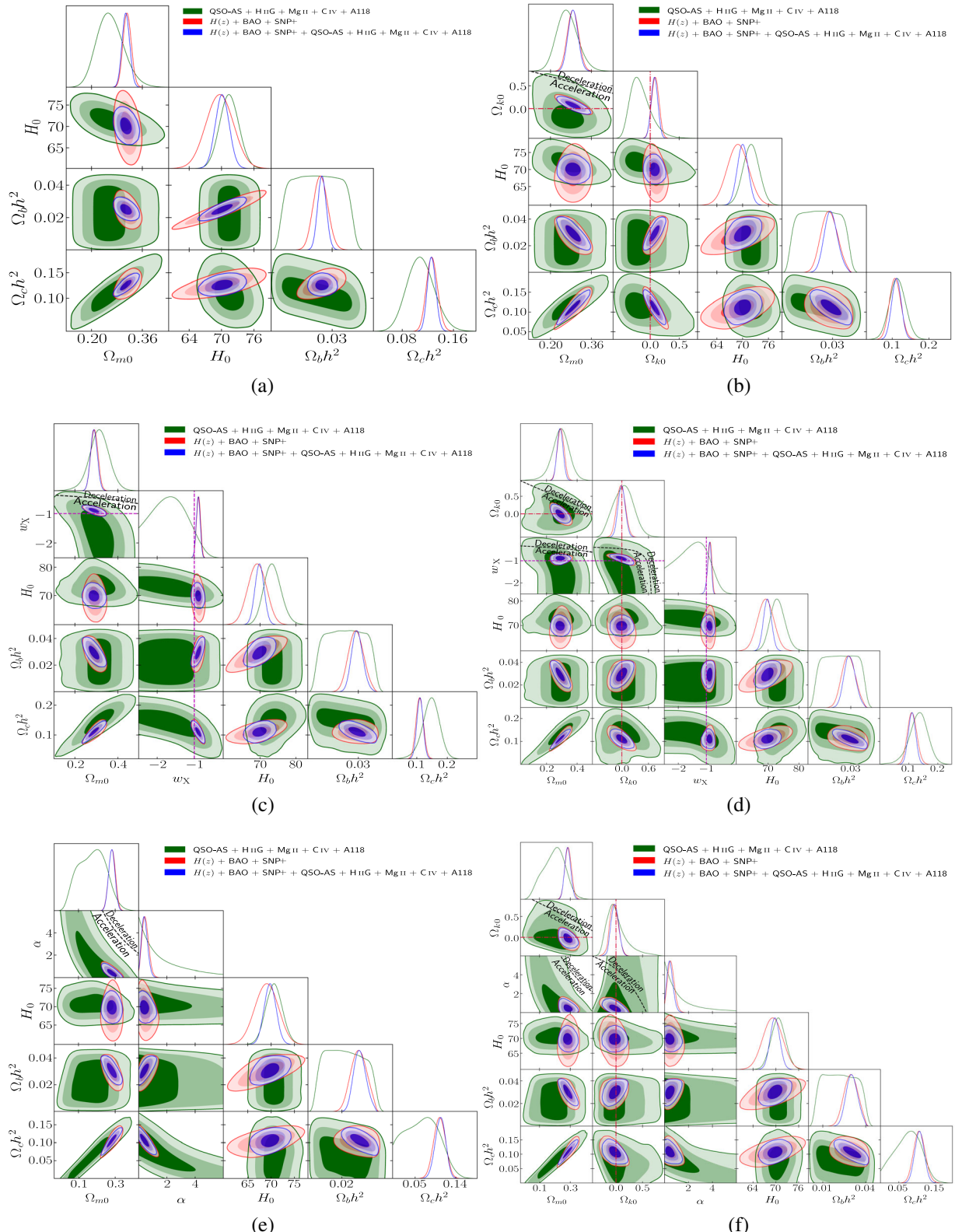


FIG. 7. Same as Fig. 1 but for QSO-AS + H_{II}G + Mg II + C IV + A118 (green), $H(z) + \text{BAO} + \text{SNP+}$ (red), and $H(z) + \text{BAO} + \text{SNP+} + \text{QSO-AS} + \text{H}_\text{II}G + \text{Mg II} + \text{C IV} + \text{A118}$ (blue) data. The black dashed zero-acceleration lines in panels (b)–(f), computed for the third cosmological parameter set to the $H(z) + \text{BAO}$ data best-fitting values listed in Table IV in panels (d) and (f), divides the parameter space into regions associated with currently accelerating (below or below left) and currently decelerating (above or above right) cosmological expansion.

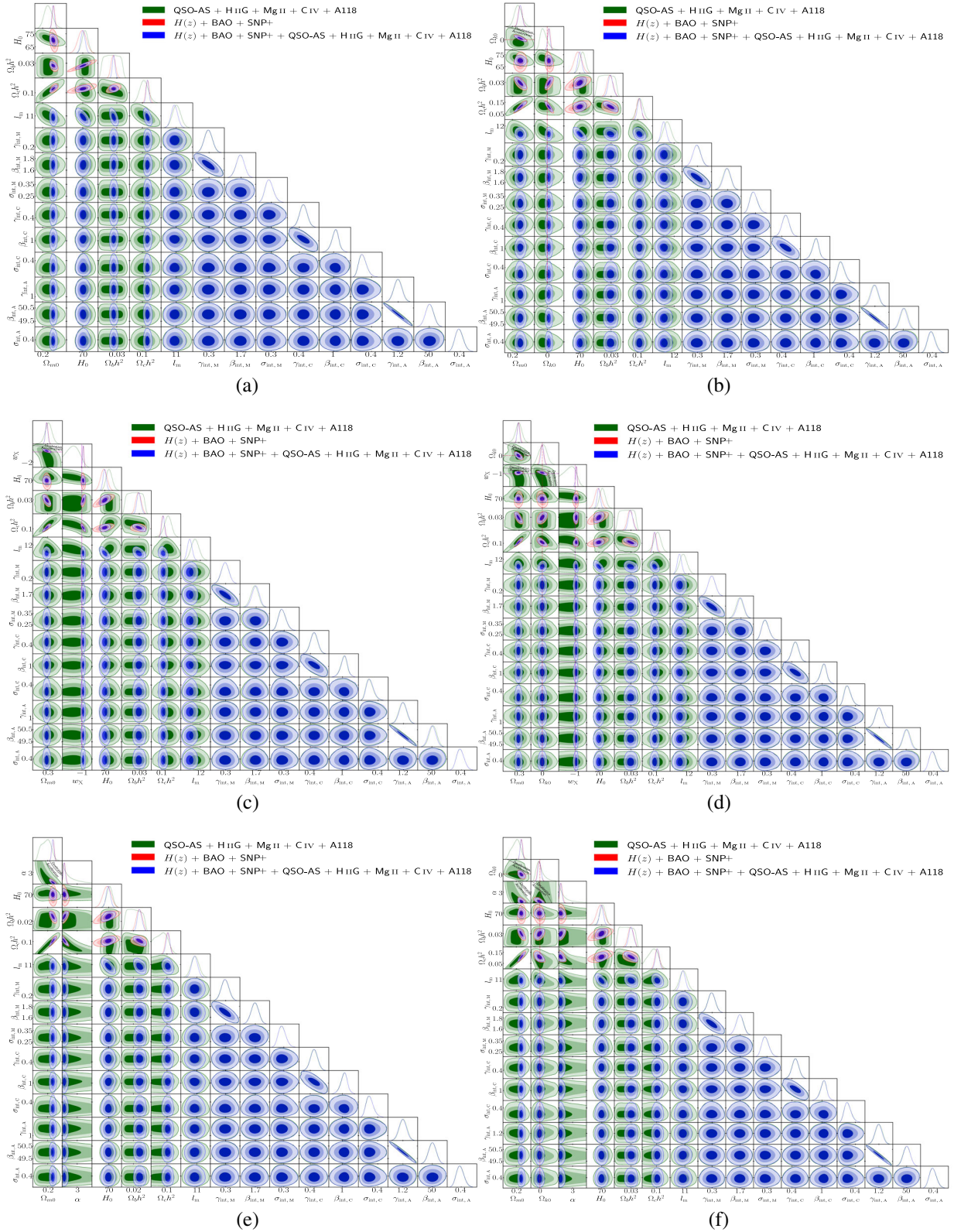


FIG. 8. Same as Fig. 7 but including noncosmological parameters.

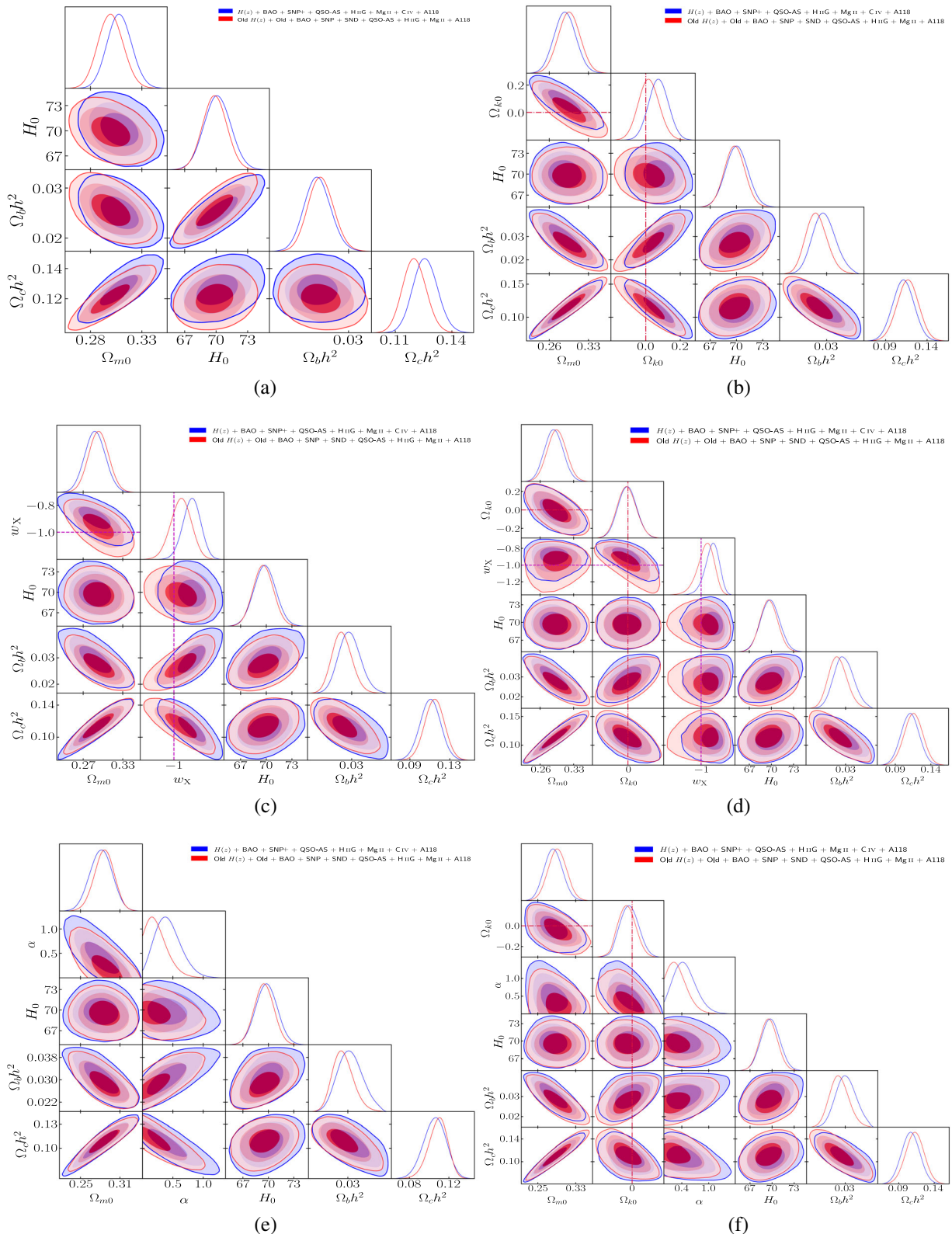


FIG. 9. Same as Fig. 1 but for old $H(z) +$ old BAO + QSO-AS + HIIg + MgII + A118 (red) and $H(z) +$ BAO + SNP + +QSO-AS + HIIg + MgII + CIV + A118 (blue) data.

against flat XCDM is positive, against nonflat Λ CDM is strong, and against other models/parametrizations are very strong.

- (ii) *BIC.* $H(z)$ +BAO data favor flat ϕ CDM the most, Mg II + C IV favor nonflat XCDM the most, and the other data combinations favor flat Λ CDM the most.

$H(z)$ +BAO and $H(z)$ +BAO+SNP+ data provide only weak or positive evidence against other models/parametrizations.

$H(z)$, QSO-AS + H II G, and A118 data provide positive or strong (nonflat XCDM and nonflat ϕ CDM) evidence against other models/parametrizations.

Mg II + C IV data provide positive evidence against nonflat Λ CDM and flat XCDM, strong evidence against flat Λ CDM, and very strong evidence against flat and nonflat ϕ CDM.

SNP+ data provide strong or very strong (nonflat XCDM and nonflat ϕ CDM) evidence against other models/parametrizations.

QHMCA data provide positive evidence against nonflat Λ CDM and flat XCDM, strong evidence against flat ϕ CDM, and very strong evidence against nonflat XCDM and nonflat ϕ CDM.

HzBSNQHMCA data provide positive or very strong (nonflat XCDM and nonflat ϕ CDM) evidence against other models/parametrizations.

- (iii) *DIC.* Mg II + C IV data favor flat XCDM the most, $H(z)$ +BAO, $H(z)$ +BAO+SNP+, A118, and HzBSNQHMCA data favor flat ϕ CDM the most, and the other data combinations favor flat Λ CDM the most.

There is strong evidence against nonflat XCDM and nonflat ϕ CDM from QSO-AS + H II G data, strong evidence against nonflat ϕ CDM from QHMCA data, and weak or positive evidence against the others from the remaining datasets.

Based on the more reliable DIC values, we conclude that HzBSNQHMCA data do not provide strong evidence against any of the considered cosmological models and parametrizations, and that this is also the case based on DIC values for the more standard HzBSN data.

VI. CONCLUSION

We have used a large compilation of available lower-redshift, non-CMB, expansion-rate datasets to derive cosmological constraints. By analyzing 32 $H(z)$, 12 BAO, 1590 Pantheon + SN Ia (SNP+), 120 QSO-AS, 181 H II G, 78 Mg II QSO, 38 C IV QSO, and 118 A118 GRB measurements, we find that the results from each individual dataset are mutually consistent, and so these data can be jointly used to study cosmological models. Additionally, we compare these new dataset constraints to their older counterparts and do not find large differences.

The $H(z)$ +BAO+SNP++QSO-AS+H II G+Mg II+C IV+A118 (HzBSNQHMCA) data combination results in a fairly precise summary value of $\Omega_{m0} = 0.288 \pm 0.017$ (very similar to the $\Omega_{m0} = 0.295 \pm 0.017$ we found in Ref. [58]), which is in agreement with many recent measurements, e.g., Ref. [139], and summary values of $\Omega_b h^2 = 0.0294 \pm 0.0036$ and $\Omega_b h^2 = 0.1107 \pm 0.0113$. Our summary value of the Hubble constant, $H_0 = 69.8 \pm 1.3 \text{ km s}^{-1} \text{ Mpc}^{-1}$ (very similar to the $H_0 = 69.7 \pm 1.2 \text{ km s}^{-1} \text{ Mpc}^{-1}$ we found in Ref. [58]), is more in line with the values reported in Refs. [59,60] than with the result of Ref. [61]. Specifically, our summary central value of H_0 matches that of Ref. [60], and is 0.58σ higher and 1.9σ lower than the values reported in Refs. [59,61], respectively. Similar to the approach outlined in Refs. [16,58,140], the summary central value is the average of the two (of six model) central mean values, while the uncertainties are the quadrature sum of the systematic uncertainty, defined as half of the difference between the two central mean values, and the statistical uncertainty, defined as the average of the error bars of the two central results. We note that from model to model the Ω_{m0} and $\Omega_b h^2$ values range over 1.3σ , while those of $\Omega_c h^2$ range over 1.5σ , unlike the H_0 values which range over only 0.21σ .

Our flat Λ CDM HzBSNQHMCA constraints, $\Omega_b h^2 = 0.0250 \pm 0.0021$, $\Omega_c h^2 = 0.1260 \pm 0.0064$, $H_0 = 70.13 \pm 1.25 \text{ km s}^{-1} \text{ Mpc}^{-1}$, and $\Omega_{m0} = 0.308 \pm 0.012$, are 1.2σ , 0.92σ , and 2.0σ higher, and 0.52σ lower than those from *Planck* TT, TE, EE + lowE + lensing CMB anisotropy data, $\Omega_b h^2 = 0.02237 \pm 0.00015$, $\Omega_c h^2 = 0.1200 \pm 0.0012$, $H_0 = 67.36 \pm 0.54 \text{ km s}^{-1} \text{ Mpc}^{-1}$, and $\Omega_{m0} = 0.3153 \pm 0.0073$, [7], where our uncertainties are 14, 5.3, 2.3, and 1.6 times larger than those from *Planck* data, respectively. Our summary values of $\Omega_b h^2$, $\Omega_c h^2$, H_0 , and Ω_{m0} , are 2.0σ higher, 0.82σ lower, 1.7σ higher, and 1.5σ lower than those from flat Λ CDM *Planck* data, where our summary values uncertainties are 24, 9.4, 2.4, and 2.3 times larger than those from *Planck* data, respectively.

Our estimated error bar for H_0 is slightly larger than that of Ref. [61] but is still much (2.4 times) larger than the error bar from the flat Λ CDM model *Planck* value [7]. Our measured summary value for $H_0 = 69.8 \pm 1.3 \text{ km s}^{-1} \text{ Mpc}^{-1}$ falls between the results from the flat Λ CDM model *Planck* value, [7], and the Cepheids and SN Ia measurement of Ref. [61], differing by about 2σ from both. (As discussed in the Appendix, excluding H II G data results in H_0 values that are $\sim 0.9\sigma$ higher than the *Planck* flat Λ CDM model value and $\sim 1.3\text{--}1.6\sigma$ lower than the Cepheids and SN Ia local expansion rate value of Ref. [61].) Our H_0 value is reasonably consistent with the slightly less-constraining flat Λ CDM model Atacama Cosmology Telescope (ACT) and South Pole Telescope (SPT) CMB anisotropy values, $H_0 = 67.9 \pm 1.5 \text{ km s}^{-1} \text{ Mpc}^{-1}$ and $H_0 = 68.8 \pm 1.5 \text{ km s}^{-1} \text{ Mpc}^{-1}$, [141,142], respectively. Our measured

summary value of H_0 also agrees well with the slightly less-constraining TRGB and SN Ia measurement of Ref. [60]. These agreements might mean that $H_0 = 69.8 \pm 1.3 \text{ km s}^{-1} \text{ Mpc}^{-1}$ is the current most reasonable value for the Hubble constant.

HzBSNQHMCA data show at most mild evidence for nonflat geometry (the strongest being 1.3σ evidence for open geometry in the nonflat Λ CDM model) but indicate more significant evidence for dark energy dynamics, from 1.6σ in the nonflat models to 2σ or larger in the flat dynamical dark energy models.

The DIC analysis shows that the HzBSNQHMCA data combination supports flat ϕ CDM the most, but it does not provide strong evidence against models with constant dark energy or a small spatial curvature energy density (the evidence against them is either weak or positive).

We look forward to a future where the quality and quantity of lower-redshift, non-CMB and non-distance-ladder, expansion-rate data, such as those utilized in this study, are significantly improved to the level where they can measure cosmological parameter values with error bars comparable to those obtained from *Planck* CMB anisotropy data.

ACKNOWLEDGMENTS

We thank Dillon Brout and Javier de Cruz Pérez for useful discussions about Pantheon+ data, Ricardo Chávez and Adam Riess for useful discussions about H II G data, and Michele Moresco and Adam Riess for encouraging us to account for $H(z)$ correlations. We also acknowledge valuable comments from Jim Peebles and Adam Riess. This research was supported in part by DOE Grant No. DE-SC0011840. The computations for this project were performed on the Beocat Research Cluster at Kansas State University, which is funded in part by NSF Grants No. CNS-1006860, No. EPS-1006860, No. EPS-0919443, No. ACI-1440548, No. CHE-1726332, and No. NIH P20GM113109.

APPENDIX: CONSTRAINTS FROM $H(z) + \text{BAO} + \text{SNP} + \text{QSO-AS} +$ $\text{Mg II} + \text{C IV} + \text{A118}$ DATA

For $H(z) + \text{BAO} + \text{SNP} + \text{QSO-AS} + \text{Mg II} + \text{C IV} + \text{A118}$ (HzBSNQMCA) data, the best-fitting parameter values, likelihood values, and information criteria values for all models are given in Table VI, and the marginalized

posterior mean parameter values and uncertainties for all models are listed in Table VII. These results are independent of both CMB data and local distance-ladder data, such as the Cepheid or TRGB distances.

The results presented in Fig. 10 suggest that the differences between the HzBSN and HzBSNQMCA data constraints are relatively small. Furthermore, the comparison of the one-dimensional marginalized constraints from the two datasets supports this conclusion. Specifically, the central values of Ω_{m0} derived from HzBSNQMCA data are only $0.057\text{--}0.17\sigma$ higher than those obtained from HzBSN data, with error bars $4.8\%\text{--}7.7\%$ smaller, except that in the flat XCDM case the error bars are similar.

The central values of Ω_{k0} derived from HzBSNQMCA data are 0.16σ , 0.12σ , and 0.083σ lower than those obtained from HzBSN data, with error bars 6.3% , 11% , and 5.1% smaller, for nonflat Λ CDM, XCDM, and ϕ CDM respectively.

The central values of H_0 derived from HzBSNQMCA data are from 0.043σ lower to 0.0085σ (nonflat XCDM and ϕ CDM) higher than those obtained from HzBSN data, with error bars $1.6\%\text{--}4.8\%$ smaller, except that in the nonflat Λ CDM case the error bar is 0.41% larger.

Similar to HzBSN H_0 constraints, HzBSNQMCA data H_0 constraints range from $68.88 \pm 2.45 \text{ km s}^{-1} \text{ Mpc}^{-1}$ (nonflat Λ CDM) to $69.50^{+2.45}_{-2.44} \text{ km s}^{-1} \text{ Mpc}^{-1}$ (flat Λ CDM), with a difference of 0.18σ . These H_0 values are 0.24σ (nonflat Λ CDM) and 0.40σ (flat Λ CDM) higher than the median statistics estimate of $H_0 = 68 \pm 2.8 \text{ km s}^{-1} \text{ Mpc}^{-1}$ [59], 0.31σ (nonflat Λ CDM) and 0.10σ (flat Λ CDM) lower than the TRGB and SN Ia estimate of $H_0 = 69.8 \pm 1.7 \text{ km s}^{-1} \text{ Mpc}^{-1}$ [60], and 1.6σ (nonflat Λ CDM) and 1.3σ (flat Λ CDM) lower than the Cepheids and SN Ia measurement of $73.04 \pm 1.04 \text{ km s}^{-1} \text{ Mpc}^{-1}$ [61]. The H_0 constraints from flat Λ CDM is 0.86σ higher than the H_0 estimate of $67.36 \pm 0.54 \text{ km s}^{-1} \text{ Mpc}^{-1}$ from *Planck* 2018 TT, TE, EE + lowE + lensing CMB anisotropy data [7].

The central values of w_X derived from HzBSNQMCA data are 0.040σ lower and 0.072σ higher than those obtained from HzBSN data, with error bars 1.9% and 8.6% smaller, for flat and nonflat XCDM, respectively. The central values of α derived from HzBSNQMCA data are 0.079σ and 0.018σ lower than those obtained from HzBSN data, with error bars 5.9% and 2.0% smaller, for flat and nonflat ϕ CDM, respectively.

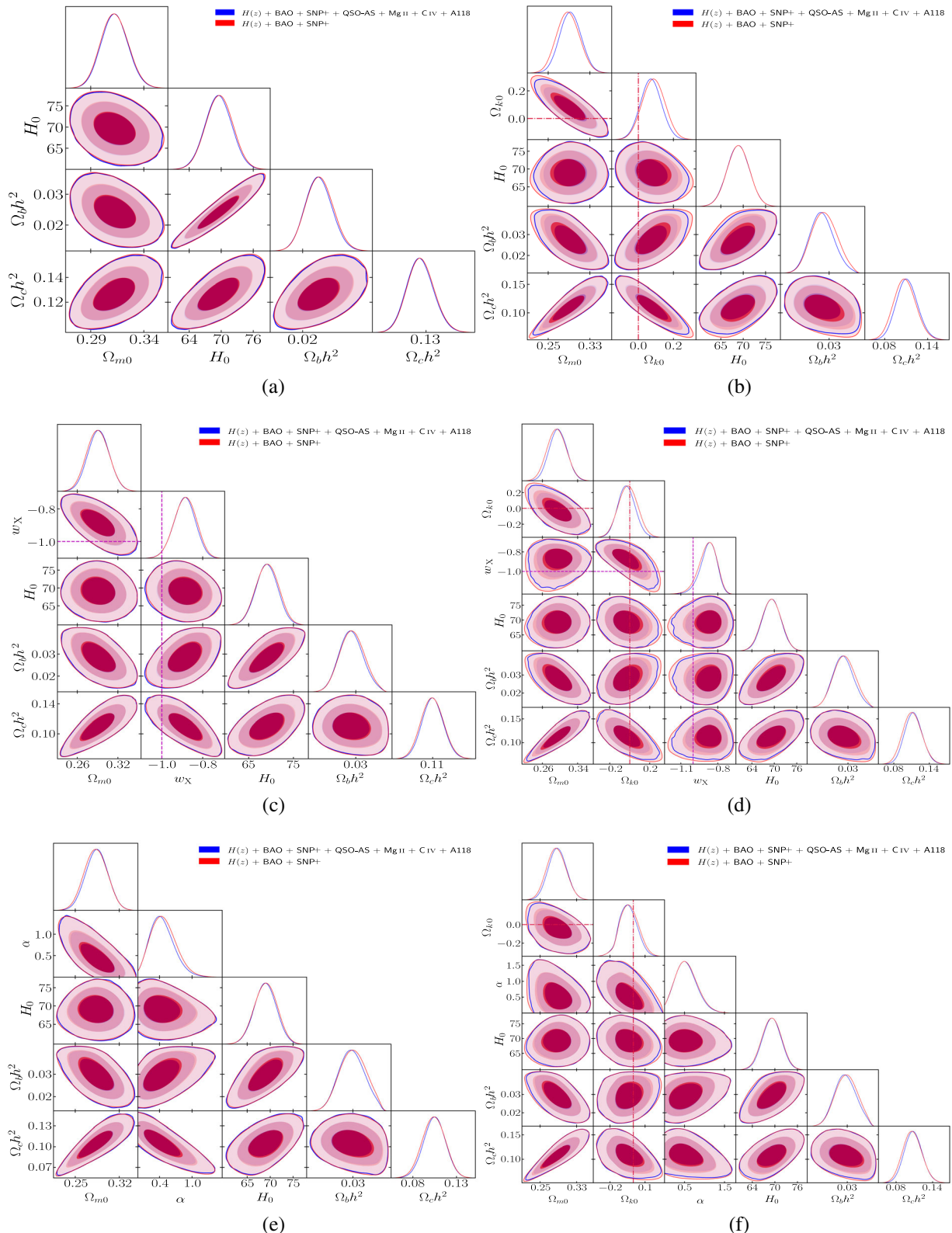


FIG. 10. Same as Fig. 1 but for $H(z)+\text{BAO}+\text{SNP+}+\text{QSO-AS}+\text{Mg II}+\text{C IV}+\text{A118}$ (blue) and $H(z)+\text{BAO}+\text{SNP+}$ (red) data.

- [1] P. J. E. Peebles, Tests of cosmological models constrained by inflation, *Astrophys. J.* **284**, 439 (1984).
- [2] E. Di Valentino, O. Mena, S. Pan, L. Visinelli, W. Yang, A. Melchiorri, D. F. Mota, A. G. Riess, and J. Silk, In the realm of the Hubble tension—a review of solutions, *Classical Quantum Gravity* **38**, 153001 (2021).
- [3] L. Perivolaropoulos and F. Skara, Challenges for Λ CDM: An update, *New Astron. Rev.* **95**, 101659 (2022).
- [4] M. Moresco, L. Amati, L. Amendola, S. Birrer, J. P. Blakeslee, M. Cantiello, A. Cimatti, J. Darling, M. Della Valle, M. Fishbach *et al.*, Unveiling the Universe with emerging cosmological probes, *Living Rev. Relativity* **25**, 6 (2022).
- [5] E. Abdalla, G. F. Abellán, A. Aboubrahim, A. Agnello, Ö. Akarsu, Y. Akrami, G. Alesta, D. Aloni, L. Amendola, L. A. Anchordoqui *et al.*, Cosmology intertwined: A review of the particle physics, astrophysics, and cosmology associated with the cosmological tensions and anomalies, *J. High Energy Astrophys.* **34**, 49 (2022).
- [6] J.-P. Hu and F.-Y. Wang, Hubble tension: The evidence of new physics, *Universe* **9**, 94 (2023).
- [7] Planck Collaboration, Planck 2018 results. VI. Cosmological parameters, *Astron. Astrophys.* **641**, A6 (2020).
- [8] H. Yu, B. Ratra, and F.-Y. Wang, Hubble parameter and baryon acoustic oscillation measurement constraints on the Hubble constant, the deviation from the spatially flat Λ CDM model, the deceleration-acceleration transition redshift, and spatial curvature, *Astrophys. J.* **856**, 3 (2018).
- [9] EBOSS Collaboration, Completed SDSS-IV extended baryon oscillation spectroscopic survey: Cosmological implications from two decades of spectroscopic surveys at the Apache point observatory, *Phys. Rev. D* **103**, 083533 (2021).
- [10] D. Brout, D. Scolnic, B. Popovic, A. G. Riess, A. Carr, J. Zuntz, R. Kessler, T. M. Davis, S. Hinton, D. Jones *et al.*, The Pantheon+ analysis: Cosmological constraints, *Astrophys. J.* **938**, 110 (2022).
- [11] D. Mania and B. Ratra, Constraints on dark energy from H II starburst galaxy apparent magnitude versus redshift data, *Phys. Lett. B* **715**, 9 (2012).
- [12] R. Chávez, R. Terlevich, E. Terlevich, F. Bresolin, J. Melnick, M. Plionis, and S. Basilakos, The L- σ relation for massive bursts of star formation, *Mon. Not. R. Astron. Soc.* **442**, 3565 (2014).
- [13] A. L. González-Morán, R. Chávez, E. Terlevich, R. Terlevich, D. Fernández-Arenas, F. Bresolin, M. Plionis, J. Melnick, S. Basilakos, and E. Telles, Independent cosmological constraints from high-z H II galaxies: New results from VLT-KMOS data, *Mon. Not. R. Astron. Soc.* **505**, 1441 (2021).
- [14] J. P. Johnson, A. Sangwan, and S. Shankaranarayanan, Observational constraints and predictions of the interacting dark sector with field-fluid mapping, *J. Cosmol. Astropart. Phys.* **01** (2022) 024.
- [15] A. Mehrabi, S. Basilakos, P. Tsipari, M. Plionis, R. Terlevich, E. Terlevich, A. L. Gonzalez Moran, R. Chavez, F. Bresolin, D. Fernandez Arenas, and E. Telles, Using our newest VLT-KMOS HII galaxies and other cosmic tracers to test the Lambda cold dark matter tension, *Mon. Not. R. Astron. Soc.* **509**, 224 (2022).
- [16] S. Cao, J. Ryan, and B. Ratra, Cosmological constraints from H II starburst galaxy, quasar angular size, and other measurements, *Mon. Not. R. Astron. Soc.* **509**, 4745 (2022).
- [17] S. Cao, X. Zheng, M. Biesiada, J. Qi, Y. Chen, and Z.-H. Zhu, Ultra-compact structure in intermediate-luminosity radio quasars: building a sample of standard cosmological rulers and improving the dark energy constraints up to z 3, *Astron. Astrophys.* **606**, A15 (2017).
- [18] J. Ryan, Y. Chen, and B. Ratra, Baryon acoustic oscillation, Hubble parameter, and angular size measurement constraints on the Hubble constant, dark energy dynamics, and spatial curvature, *Mon. Not. R. Astron. Soc.* **488**, 3844 (2019).
- [19] S. Cao, J. Ryan, and B. Ratra, Cosmological constraints from HII starburst galaxy apparent magnitude and other cosmological measurements, *Mon. Not. R. Astron. Soc.* **497**, 3191 (2020).
- [20] X. Zheng, S. Cao, M. Biesiada, X. Li, T. Liu, and Y. Liu, Multiple measurements of quasars acting as standard probes: Model independent calibration and exploring the dark energy equation of states, *Sci. China Phys. Mech. Astron.* **64**, 259511 (2021).
- [21] Y. Lian, S. Cao, M. Biesiada, Y. Chen, Y. Zhang, and W. Guo, Probing modified gravity theories with multiple measurements of high-redshift quasars, *Mon. Not. R. Astron. Soc.* **505**, 2111 (2021).
- [22] B. Czerny, M. L. Martínez-Aldama, G. Wojtkowska, M. Zajaček, P. Marziani, D. Dultzin, M. H. Naddaf, S. Panda, R. Prince, R. Przyłuski, M. Ralowski, and M. Śniegowska, Dark energy constraints from quasar observations, *Acta Phys. Pol. A* **139**, 389 (2021).
- [23] M. Zajaček, B. Czerny, M. L. Martinez-Aldama, M. Rałowski, A. Olejak, R. Przyłuski, S. Panda, K. Hryniewicz, M. Śniegowska, M.-H. Naddaf *et al.*, Time delay of Mg II emission response for the luminous quasar HE 0435-4312: Toward application of the high-accretor radius-luminosity relation in cosmology, *Astrophys. J.* **912**, 10 (2021).
- [24] Z. Yu, P. Martini, A. Penton, T. M. Davis, U. Malik, C. Lidman, B. E. Tucker, R. Sharp, C. S. Kochanek, B. M. Peterson *et al.*, OzDES reverberation mapping programme: The first Mg II lags from 5 yr of monitoring, *Mon. Not. R. Astron. Soc.* **507**, 3771 (2021).
- [25] N. Khadka, Z. Yu, M. Zajaček, M. L. Martinez-Aldama, B. Czerny, and B. Ratra, Standardizing reverberation-measured Mg II time-lag quasars, by using the radius-luminosity relation, and constraining cosmological model parameters, *Mon. Not. R. Astron. Soc.* **508**, 4722 (2021).
- [26] N. Khadka, M. Zajaček, S. Panda, M. L. Martínez-Aldama, and B. Ratra, Consistency study of high- and low-accreting Mg II quasars: No significant effect of the Fe II to Mg II flux ratio on the radius–luminosity relation dispersion, *Mon. Not. R. Astron. Soc.* **515**, 3729 (2022).
- [27] S. Cao, M. Zajaček, S. Panda, M. L. Martínez-Aldama, B. Czerny, and B. Ratra, Standardizing reverberation-measured C IV time-lag quasars, and using them with standardized Mg II quasars to constrain cosmological parameters, *Mon. Not. R. Astron. Soc.* **516**, 1721 (2022).

- [28] B. Czerny *et al.*, Accretion disks, quasars and cosmology: Meandering towards understanding, *Astrophys. Space Sci.* **368**, 8 (2023).
- [29] J. S. Wang, F. Y. Wang, K. S. Cheng, and Z. G. Dai, Measuring dark energy with the $E_{\text{iso}}\text{-}E_p$ correlation of gamma-ray bursts using model-independent methods, *Astron. Astrophys.* **585**, A68 (2016).
- [30] F. Fana Dirirsa, S. Razzaque, F. Piron, M. Arimoto, M. Axelsson, D. Kocevski, F. Longo, M. Ohno, and S. Zhu, Spectral analysis of fermi-LAT gamma-ray bursts with known redshift and their potential use as cosmological standard candles, *Astrophys. J.* **887**, 13 (2019).
- [31] N. Khadka and B. Ratra, Constraints on cosmological parameters from gamma-ray burst peak photon energy and bolometric fluence measurements and other data, *Mon. Not. R. Astron. Soc.* **499**, 391 (2020).
- [32] S. Cao, J. Ryan, N. Khadka, and B. Ratra, Cosmological constraints from higher-redshift gamma-ray burst, H II starburst galaxy, and quasar (and other) data, *Mon. Not. R. Astron. Soc.* **501**, 1520 (2021).
- [33] M. G. Dainotti, A. L. Lenart, G. Sarracino, S. Nagataki, S. Capozziello, and N. Fraija, The x-ray fundamental plane of the platinum sample, the kilonovae, and the SNe Ib/c associated with GRBs, *Astrophys. J.* **904**, 97 (2020).
- [34] J. P. Hu, F. Y. Wang, and Z. G. Dai, Measuring cosmological parameters with a luminosity-time correlation of gamma-ray bursts, *Mon. Not. R. Astron. Soc.* **507**, 730 (2021).
- [35] Y. Dai, X.-G. Zheng, Z.-X. Li, H. Gao, and Z.-H. Zhu, Redshift evolution of the Amati relation: Calibrated results from the Hubble diagram of quasars at high redshifts, *Astron. Astrophys.* **651**, L8 (2021).
- [36] M. Demianski, E. Piedipalumbo, D. Sawant, and L. Amati, Prospects of high redshift constraints on dark energy models with the $E_{p,i}\text{-}E_{\text{iso}}$ correlation in long gamma ray bursts, *Mon. Not. R. Astron. Soc.* **506**, 903 (2021).
- [37] N. Khadka, O. Luongo, M. Muccino, and B. Ratra, Do gamma-ray burst measurements provide a useful test of cosmological models?, *J. Cosmol. Astropart. Phys.* **09** (2021) 042.
- [38] S. Cao, M. Dainotti, and B. Ratra, Gamma-ray burst data strongly favour the three-parameter fundamental plane (Dainotti) correlation over the two-parameter one, *Mon. Not. R. Astron. Soc.* **516**, 1386 (2022).
- [39] M. G. Dainotti, V. Nielson, G. Sarracino, E. Rinaldi, S. Nagataki, S. Capozziello, O. Y. Gnedin, and G. Bargiacchi, Optical and x-ray GRB fundamental planes as cosmological distance indicators, *Mon. Not. R. Astron. Soc.* **514**, 1828 (2022).
- [40] O. Luongo and M. Muccino, A roadmap to gamma-ray bursts: New developments and applications to cosmology, *Galaxies* **9**, 77 (2021).
- [41] S. Cao, N. Khadka, and B. Ratra, Standardizing Dainotti-correlated gamma-ray bursts, and using them with standardized Amati-correlated gamma-ray bursts to constrain cosmological model parameters, *Mon. Not. R. Astron. Soc.* **510**, 2928 (2022).
- [42] S. Cao, M. Dainotti, and B. Ratra, Standardizing Platinum Dainotti-correlated gamma-ray bursts, and using them with standardized Amati-correlated gamma-ray bursts to constrain cosmological model parameters, *Mon. Not. R. Astron. Soc.* **512**, 439 (2022).
- [43] Y. Liu, F. Chen, N. Liang, Z. Yuan, H. Yu, and P. Wu, The improved amati correlations from gaussian copula, *Astrophys. J.* **931**, 50 (2022).
- [44] N. Khadka, M. L. Martínez-Aldama, M. Zajaček, B. Czerny, and B. Ratra, Do reverberation-measured $H\beta$ quasars provide a useful test of cosmology?, *Mon. Not. R. Astron. Soc.* **513**, 1985 (2022).
- [45] G. Risaliti and E. Lusso, A Hubble diagram for quasars, *Astrophys. J.* **815**, 33 (2015).
- [46] G. Risaliti and E. Lusso, Cosmological constraints from the Hubble diagram of quasars at high redshifts, *Nat. Astron.* **3**, 272 (2019).
- [47] N. Khadka and B. Ratra, Quasar X-ray and UV flux, baryon acoustic oscillation, and Hubble parameter measurement constraints on cosmological model parameters, *Mon. Not. R. Astron. Soc.* **492**, 4456 (2020).
- [48] T. Yang, A. Banerjee, and E. Ó. Colgáin, Cosmography and flat Λ CDM tensions at high redshift, *Phys. Rev. D* **102**, 123532 (2020).
- [49] N. Khadka and B. Ratra, Using quasar x-ray and UV flux measurements to constrain cosmological model parameters, *Mon. Not. R. Astron. Soc.* **497**, 263 (2020).
- [50] E. Lusso, G. Risaliti, E. Nardini, G. Bargiacchi, M. Benetti, S. Bisogni, S. Capozziello, F. Civano, L. Eggleston, M. Elvis *et al.*, Quasars as standard candles. III. Validation of a new sample for cosmological studies, *Astron. Astrophys.* **642**, A150 (2020).
- [51] N. Khadka and B. Ratra, Determining the range of validity of quasar X-ray and UV flux measurements for constraining cosmological model parameters, *Mon. Not. R. Astron. Soc.* **502**, 6140 (2021).
- [52] N. Khadka and B. Ratra, Do quasar x-ray and UV flux measurements provide a useful test of cosmological models?, *Mon. Not. R. Astron. Soc.* **510**, 2753 (2022).
- [53] M. Rezaei, J. Solà Peracaula, and M. Malekjani, Cosmographic approach to running vacuum dark energy models: New constraints using BAOs and Hubble diagrams at higher redshifts, *Mon. Not. R. Astron. Soc.* **509**, 2593 (2022).
- [54] O. Luongo, M. Muccino, E. Ó. Colgáin, M. M. Sheikh-Jabbari, and L. Yin, Larger H_0 values in the CMB dipole direction, *Phys. Rev. D* **105**, 103510 (2022).
- [55] M. G. Dainotti, G. Bargiacchi, A. L. Lenart, S. Capozziello, E. Ó Colgáin, R. Solomon, D. Stojkovic, and M. M. Sheikh-Jabbari, Quasar standardization: Overcoming selection biases and redshift evolution, *Astrophys. J.* **931**, 106 (2022).
- [56] V. Petrosian, J. Singal, and S. Mutchnick, Can the distance-redshift relation be determined from correlations between luminosities?, *Astrophys. J. Lett.* **935**, L19 (2022).
- [57] N. Khadka, M. Zajaček, R. Prince, S. Panda, B. Czerny, M. L. Martínez-Aldama, V. K. Jaiswal, and B. Ratra, Quasar UV/X-ray relation luminosity distances are shorter than reverberation-measured radius-luminosity relation luminosity distances, *Mon. Not. R. Astron. Soc.* **522**, 1247 (2023).
- [58] S. Cao and B. Ratra, Using lower redshift, non-CMB, data to constrain the Hubble constant and other cosmological parameters, *Mon. Not. R. Astron. Soc.* **513**, 5686 (2022).

- [59] G. Chen and B. Ratra, Median statistics and the Hubble constant, *Publ. Astron. Soc. Pac.* **123**, 1127 (2011).
- [60] W. L. Freedman, Measurements of the Hubble constant: Tensions in perspective, *Astrophys. J.* **919**, 16 (2021).
- [61] A. G. Riess, W. Yuan, L. M. Macri, D. Scolnic, D. Brout, S. Casertano, D. O. Jones, Y. Murakami, G. S. Anand, L. Breuval *et al.*, A comprehensive measurement of the local value of the Hubble constant with $1 \text{ km s}^{-1} \text{ Mpc}^{-1}$ uncertainty from the Hubble space telescope and the SH0ES team, *Astrophys. J. Lett.* **934**, L7 (2022).
- [62] A. Rana, D. Jain, S. Mahajan, and A. Mukherjee, Constraining cosmic curvature by using age of galaxies and gravitational lenses, *J. Cosmol. Astropart. Phys.* **03** (2017) 028.
- [63] J. Ooba, B. Ratra, and N. Sugiyama, Planck 2015 constraints on the non-flat Λ CDM inflation model, *Astrophys. J.* **864**, 80 (2018).
- [64] J. Ooba, B. Ratra, and N. Sugiyama, Planck 2015 constraints on the non-flat XCDM inflation model, *Astrophys. J.* **869**, 34 (2018).
- [65] C.-G. Park and B. Ratra, Using the tilted flat- Λ CDM and the untilted non-flat Λ CDM inflation models to measure cosmological parameters from a compilation of observational data, *Astrophys. J.* **882**, 158 (2019).
- [66] C.-G. Park and B. Ratra, Observational constraints on the tilted flat-XCDM and the untilted nonflat XCDM dynamical dark energy inflation parameterizations, *Astrophys. Space Sci.* **364**, 82 (2019).
- [67] DES Collaboration, Dark energy survey year 1 results: Constraints on extended cosmological models from galaxy clustering and weak lensing, *Phys. Rev. D* **99**, 123505 (2019).
- [68] E.-K. Li, M. Du, and L. Xu, General cosmography model with spatial curvature, *Mon. Not. R. Astron. Soc.* **491**, 4960 (2020).
- [69] G. Efstathiou and S. Gratton, The evidence for a spatially flat Universe, *Mon. Not. R. Astron. Soc.* **496**, L91 (2020).
- [70] E. Di Valentino, A. Melchiorri, and J. Silk, Investigating cosmic discordance, *Astrophys. J. Lett.* **908**, L9 (2021).
- [71] KiDS Collaboration, KiDS-1000 Cosmology: Constraints beyond flat Λ CDM, *Astron. Astrophys.* **649**, A88 (2021).
- [72] S. Vagnozzi, A. Loeb, and M. Moresco, Eppur è piatto? The cosmic chronometers take on spatial curvature and cosmic concordance, *Astrophys. J.* **908**, 84 (2021).
- [73] R. Arjona and S. Nesseris, Novel null tests for the spatial curvature and homogeneity of the Universe and their machine learning reconstructions, *Phys. Rev. D* **103**, 103539 (2021).
- [74] S. Dhawan, J. Alsing, and S. Vagnozzi, Non-parametric spatial curvature inference using late-Universe cosmological probes, *Mon. Not. R. Astron. Soc.: Lett.* **506**, L1 (2021).
- [75] F. Renzi, N. B. Hogg, and W. Giarè, The resilience of the Etherington-Hubble relation, *Mon. Not. R. Astron. Soc.* **513**, 4004 (2022).
- [76] C.-Q. Geng, Y.-T. Hsu, and J.-R. Lu, Cosmological constraints on nonflat exponential f(R) gravity, *Astrophys. J.* **926**, 74 (2022).
- [77] J.-J. Wei and F. Melia, Exploring the Hubble tension and spatial curvature from the ages of old astrophysical objects, *Astrophys. J.* **928**, 165 (2022).
- [78] P. Mukherjee and N. Banerjee, Constraining the curvature density parameter in cosmology, *Phys. Rev. D* **105**, 063516 (2022).
- [79] A. Glanville, C. Howlett, and T. M. Davis, Full-shape galaxy power spectra and the curvature tension, *Mon. Not. R. Astron. Soc.* **517**, 3087 (2022).
- [80] Q. Wu, G.-Q. Zhang, and F.-Y. Wang, An 8 per cent determination of the Hubble constant from localized fast radio bursts, *Mon. Not. R. Astron. Soc.* **515**, L1 (2022).
- [81] J. de Cruz Perez, C.-G. Park, and B. Ratra, Current data are consistent with flat spatial hypersurfaces in the Λ CDM cosmological model but favor more lensing than the model predicts, *Phys. Rev. D* **107**, 063522 (2023).
- [82] D. Dahiya and D. Jain, Revisiting the epoch of cosmic acceleration, [arXiv:2212.04751](https://arxiv.org/abs/2212.04751).
- [83] J. Stevens, H. Khoramnezhad, and S. Saito, Constraining the spatial curvature with cosmic expansion history in a cosmological model with a non-standard sound horizon, [arXiv:2212.09804](https://arxiv.org/abs/2212.09804).
- [84] A. Favale, A. Gómez-Valent, and M. Migliaccio, Cosmic chronometers to calibrate the ladders and measure the curvature of the Universe. A model-independent study, [arXiv:2301.09591](https://arxiv.org/abs/2301.09591).
- [85] J. Solà Peracaula, A. Gómez-Valent, J. de Cruz Perez, and C. Moreno-Pulido, Running vacuum against the H_0 and σ_8 tensions, *Europhys. Lett.* **134**, 19001 (2021).
- [86] J. de Cruz Perez, J. Sola Peracaula, and C. P. Singh, Running vacuum in Brans-Dicke theory: A possible cure for the σ_8 and H_0 tensions, [arXiv:2302.04807](https://arxiv.org/abs/2302.04807).
- [87] J. Sola Peracaula, A. Gomez-Valent, J. de Cruz Perez, and C. Moreno-Pulido, Running vacuum in the Universe: Phenomenological status in light of the latest observations, and its impact on the σ_8 and H_0 tensions, [arXiv:2304.11157](https://arxiv.org/abs/2304.11157).
- [88] P. J. E. Peebles and B. Ratra, Cosmology with a time-variable cosmological ‘constant’, *Astrophys. J. Lett.* **325**, L17 (1988).
- [89] B. Ratra and P. J. E. Peebles, Cosmological consequences of a rolling homogeneous scalar field, *Phys. Rev. D* **37**, 3406 (1988).
- [90] A. Pavlov, S. Westmoreland, K. Saaidi, and B. Ratra, Nonflat time-variable dark energy cosmology, *Phys. Rev. D* **88**, 123513 (2013).
- [91] D. Blas, J. Lesgourgues, and T. Tram, The cosmic linear anisotropy solving system (CLASS). Part II: Approximation schemes, *J. Cosmol. Astropart. Phys.* **07** (2011) 034.
- [92] J. Sola, A. Gomez-Valent, and J. de Cruz Pérez, Dynamical dark energy: Scalar fields and running vacuum, *Mod. Phys. Lett. A* **32**, 1750054 (2017).
- [93] Z. Zhai, M. Blanton, A. Slosar, and J. Tinker, An evaluation of cosmological models from the expansion and growth of structure measurements, *Astrophys. J.* **850**, 183 (2017).
- [94] J. Ooba, B. Ratra, and N. Sugiyama, Planck 2015 constraints on the nonflat ϕ CDM inflation model, *Astrophys. J.* **866**, 68 (2018).

- [95] J. Ooba, B. Ratra, and N. Sugiyama, Planck 2015 constraints on spatially-flat dynamical dark energy models, *Astrophys. Space Sci.* **364**, 176 (2019).
- [96] C.-G. Park and B. Ratra, Observational constraints on the tilted spatially flat and the untilted nonflat ϕ CDM dynamical dark energy inflation models, *Astrophys. J.* **868**, 83 (2018).
- [97] C.-G. Park and B. Ratra, Measuring the Hubble constant and spatial curvature from supernova apparent magnitude, baryon acoustic oscillation, and Hubble parameter data, *Astrophys. Space Sci.* **364**, 134 (2019).
- [98] C.-G. Park and B. Ratra, Using SPT polarization, Planck 2015, and non-CMB data to constrain tilted spatially-flat and untilted nonflat Λ CDM, XCDM, and ϕ CDM dark energy inflation cosmologies, *Phys. Rev. D* **101**, 083508 (2020).
- [99] J. Solà Peracaula, A. Gómez-Valent, and J. de Cruz Pérez, Signs of dynamical dark energy in current observations, *Phys. Dark Universe* **25**, 100311 (2019).
- [100] A. Singh, A. Sangwan, and H. K. Jassal, Low redshift observational constraints on tachyon models of dark energy, *J. Cosmol. Astropart. Phys.* **04** (2019) 047.
- [101] L. A. Ureña-López and N. Roy, Generalized tracker quintessence models for dark energy, *Phys. Rev. D* **102**, 063510 (2020).
- [102] S. Sinha and N. Banerjee, Perturbations in a scalar field model with virtues of Λ CDM, *J. Cosmol. Astropart. Phys.* **04** (2021) 060.
- [103] T. Xu, Y. Chen, L. Xu, and S. Cao, Comparing the scalar-field dark energy models with recent observations, *Phys. Dark Universe* **36**, 101023 (2022).
- [104] J. de Cruz Perez, J. Sola Peracaula, A. Gomez-Valent, and C. Moreno-Pulido, BD- Λ CDM and Running Vacuum Models: Theoretical background and current observational status, *The Sixteenth Marcel Grossmann Meeting* (2023), pp. 1752–1769, 10.1142/9789811269776_0137.
- [105] J. F. Jesus, R. Valentim, A. A. Escobal, S. H. Pereira, and D. Benndorf, Gaussian processes reconstruction of the dark energy potential, *J. Cosmol. Astropart. Phys.* **11** (2022) 037.
- [106] A. Adil, A. Albrecht, and L. Knox, Quintessential cosmological tensions, *Phys. Rev. D* **107**, 063521 (2023).
- [107] M. Moresco, R. Jimenez, L. Verde, A. Cimatti, and L. Pozzetti, Setting the stage for cosmic chronometers. II. Impact of stellar population synthesis models systematics and full covariance matrix, *Astrophys. J.* **898**, 82 (2020).
- [108] <https://gitlab.com/mmoreesco/CCcovariance/>.
- [109] M. Moresco, A. Cimatti, R. Jimenez, L. Pozzetti, G. Zamorani, M. Bolzonella, J. Dunlop, F. Lamareille, M. Mignoli, H. Pearce *et al.*, Improved constraints on the expansion rate of the universe up to $z \sim 1.1$ from the spectroscopic evolution of cosmic chronometers, *J. Cosmol. Astropart. Phys.* **08** (2012) 006.
- [110] M. Moresco, Raising the bar: New constraints on the Hubble parameter with cosmic chronometers at $z \sim 2$., *Mon. Not. R. Astron. Soc.: Lett.* **450**, L16 (2015).
- [111] M. Moresco, L. Pozzetti, A. Cimatti, R. Jimenez, C. Maraston, L. Verde, D. Thomas, A. Citro, R. Tojeiro, and D. Wilkinson, A 6% measurement of the Hubble parameter at $z \sim 0.45$: Direct evidence of the epoch of cosmic re-acceleration, *J. Cosmol. Astropart. Phys.* **05** (2016) 014.
- [112] P. Carter, F. Beutler, W. J. Percival, C. Blake, J. Koda, and A. J. Ross, Low redshift baryon acoustic oscillation measurement from the reconstructed 6-degree field galaxy survey, *Mon. Not. R. Astron. Soc.* **481**, 2371 (2018).
- [113] H. du Mas des Bourboux, J. Rich, A. Font-Ribera, V. de Sainte Agathe, J. Farr, T. Etourneau, J.-M. Le Goff, A. Cuceu, C. Balland, J. E. Bautista *et al.*, The completed SDSS-IV extended baryon oscillation spectroscopic survey: Baryon acoustic oscillations with Ly α forests, *Astrophys. J.* **901**, 153 (2020).
- [114] H. Gil-Marín, J. E. Bautista, R. Paviot, M. Vargas-Magaña, S. de la Torre, S. Fromenteau, S. Alam, S. Ávila, E. Burtin, C.-H. Chuang *et al.*, The completed SDSS-IV extended baryon oscillation spectroscopic survey: Measurement of the BAO and growth rate of structure of the luminous red galaxy sample from the anisotropic power spectrum between redshifts 0.6 and 1.0, *Mon. Not. R. Astron. Soc.* **498**, 2492 (2020).
- [115] J. E. Bautista, R. Paviot, M. Vargas Magaña, S. de la Torre, S. Fromenteau, H. Gil-Marín, A. J. Ross, E. Burtin, K. S. Dawson, J. Hou *et al.*, The completed SDSS-IV extended baryon oscillation spectroscopic survey: Measurement of the BAO and growth rate of structure of the luminous red galaxy sample from the anisotropic correlation function between redshifts 0.6 and 1, *Mon. Not. R. Astron. Soc.* **500**, 736 (2021).
- [116] R. Neveux, E. Burtin, A. de Mattia, A. Smith, A. J. Ross, J. Hou, J. Bautista, J. Brinkmann, C.-H. Chuang, K. S. Dawson *et al.*, The completed SDSS-IV extended baryon oscillation spectroscopic survey: BAO and RSD measurements from the anisotropic power spectrum of the quasar sample between redshift 0.8 and 2.2, *Mon. Not. R. Astron. Soc.* **499**, 210 (2020).
- [117] J. Hou, A. G. Sánchez, A. J. Ross, A. Smith, R. Neveux, J. Bautista, E. Burtin, C. Zhao, R. Scoccimarro, K. S. Dawson *et al.*, The completed SDSS-IV extended baryon oscillation spectroscopic survey: BAO and RSD measurements from anisotropic clustering analysis of the quasar sample in configuration space between redshift 0.8 and 2.2, *Mon. Not. R. Astron. Soc.* **500**, 1201 (2021).
- [118] D. M. Scolnic, D. O. Jones, A. Rest, Y. C. Pan, R. Chornock, R. J. Foley, M. E. Huber, R. Kessler, G. Narayan, A. G. Riess *et al.*, The complete light-curve sample of spectroscopically confirmed SNe Ia from Pan-STARRS1 and cosmological constraints from the combined pantheon sample, *Astrophys. J.* **859**, 101 (2018).
- [119] DES Collaboration, First cosmology results using SNe Ia from the dark energy survey: Analysis, systematic uncertainties, and validation, *Astrophys. J.* **874**, 150 (2019).
- [120] A. L. González-Morán, R. Chávez, R. Terlevich, E. Terlevich, F. Bresolin, D. Fernández-Arenas, M. Plionis, S. Basilakos, J. Melnick, and E. Telles, Independent cosmological constraints from high-z H II galaxies, *Mon. Not. R. Astron. Soc.* **487**, 4669 (2019).
- [121] D. Fernández Arenas, E. Terlevich, R. Terlevich, J. Melnick, R. Chávez, F. Bresolin, E. Telles, M. Plionis, and S. Basilakos, An independent determination of the

- local Hubble constant, *Mon. Not. R. Astron. Soc.* **474**, 1250 (2018).
- [122] K. D. Gordon, G. C. Clayton, K. A. Misselt, A. U. Landolt, and M. J. Wolff, A quantitative comparison of the small magellanic cloud, large magellanic cloud, and Milky Way ultraviolet to near-infrared extinction curves, *Astrophys. J.* **594**, 279 (2003).
- [123] L. Amati, C. Guidorzi, F. Frontera, M. Della Valle, F. Finelli, R. Landi, and E. Montanari, Measuring the cosmological parameters with the $E_{p,i}$ - E_{iso} correlation of gamma-ray bursts, *Mon. Not. R. Astron. Soc.* **391**, 577 (2008).
- [124] L. Amati, F. Frontera, and C. Guidorzi, Extremely energetic Fermi gamma-ray bursts obey spectral energy correlations, *Astron. Astrophys.* **508**, 173 (2009).
- [125] C. Zhang, H. Zhang, S. Yuan, S. Liu, T.-J. Zhang, and Y.-C. Sun, Four new observational $H(z)$ data from luminous red galaxies in the Sloan Digital Sky Survey data release seven, *Res. Astron. Astrophys.* **14**, 1221 (2014).
- [126] J. Simon, L. Verde, and R. Jimenez, Constraints on the redshift dependence of the dark energy potential, *Phys. Rev. D* **71**, 123001 (2005).
- [127] A. L. Ratsimbazafy, S. I. Loubser, S. M. Crawford, C. M. Cress, B. A. Bassett, R. C. Nichol, and P. Väisänen, Age-dating luminous red galaxies observed with the southern african large telescope, *Mon. Not. R. Astron. Soc.* **467**, 3239 (2017).
- [128] D. Stern, R. Jimenez, L. Verde, M. Kamionkowski, and S. A. Stanford, Cosmic chronometers: Constraining the equation of state of dark energy. I: $H(z)$ measurements, *J. Cosmol. Astropart. Phys.* **02** (2010) 008.
- [129] N. Borghi, M. Moresco, and A. Cimatti, Toward a better understanding of cosmic chronometers: A new measurement of $H(z)$ at $z \sim 0.7$, *Astrophys. J. Lett.* **928**, L4 (2022).
- [130] DES Collaboration, Dark energy survey year 3 results: A 2.7% measurement of baryon acoustic oscillation distance scale at redshift 0.835, *Phys. Rev. D* **105**, 043512 (2022).
- [131] DES Collaboration, Dark energy survey year 1 results: Measurement of the baryon acoustic oscillation scale in the distribution of galaxies to redshift 1, *Mon. Not. R. Astron. Soc.* **483**, 4866 (2019).
- [132] G. D'Agostini, Fits, and especially linear fits, with errors on both axes, extra variance of the data points and other complications, [arXiv:physics/0511182](https://arxiv.org/abs/physics/0511182).
- [133] A. Conley, J. Guy, M. Sullivan, N. Regnault, P. Astier, C. Balland, S. Basa, R. G. Carlberg, D. Fouchez, D. Hardin *et al.*, Supernova constraints and systematic uncertainties from the first three years of the supernova legacy survey, *Astrophys. J. Suppl. Ser.* **192**, 1 (2011).
- [134] B. Audren, J. Lesgourgues, K. Benabed, and S. Prunet, Conservative constraints on early cosmology with MontePython, *J. Cosmol. Astropart. Phys.* **02** (2013) 001.
- [135] T. Brinckmann and J. Lesgourgues, MontePython 3: Boosted MCMC sampler and other features, *Phys. Dark Universe* **24**, 100260 (2019).
- [136] A. Lewis, GetDist: A PYTHON package for analysing Monte Carlo samples, [arXiv:1910.13970](https://arxiv.org/abs/1910.13970).
- [137] J. R. Gott, III, M. S. Vogeley, S. Podariu, and B. Ratra, Median statistics, H_0 , and the accelerating universe, *Astrophys. J.* **549**, 1 (2001).
- [138] E. Calabrese, M. Archidiacono, A. Melchiorri, and B. Ratra, Impact of H_0 prior on the evidence for dark radiation, *Phys. Rev. D* **86**, 043520 (2012).
- [139] Q. Hang, S. Alam, J. A. Peacock, and Y.-C. Cai, Galaxy clustering in the DESI Legacy Survey and its imprint on the CMB, *Mon. Not. R. Astron. Soc.* **501**, 1481 (2021).
- [140] S. Cao, J. Ryan, and B. Ratra, Using Pantheon and DES supernova, baryon acoustic oscillation, and Hubble parameter data to constrain the Hubble constant, dark energy dynamics, and spatial curvature, *Mon. Not. R. Astron. Soc.* **504**, 300 (2021).
- [141] S. Aiola, E. Calabrese, L. Maurin, S. Naess, B. L. Schmitt, M. H. Abitbol, G. E. Addison, P. A. R. Ade, D. Alonso, M. Amiri *et al.*, The Atacama cosmology telescope: DR4 maps and cosmological parameters, *J. Cosmol. Astropart. Phys.* **012** (2020) 047.
- [142] D. Dutcher, L. Balkenhol, P. A. R. Ade, Z. Ahmed, E. Anderes, A. J. Anderson, M. Archipley, J. S. Avva, K. Aylor, P. S. Barry *et al.*, Measurements of the E-mode polarization and temperature-E-mode correlation of the CMB from SPT-3G 2018 data, *Phys. Rev. D* **104**, 022003 (2021).